

TekTonika



Crustal to Microscale Strain Partitioning during Transpression and Control on Ore Formation: Insights from the Paleoproterozoic Séguéla Shear Zone, Southern West African Craton

Julien Perret (10 *1,2), Nicolas Thébaud (10 11, Denis Fougerouse (10 22), Crystal Brochard (10 32), Patrick C. Hayman (10 42), Mark W. Jessell (10 11)

¹Centre for Exploration Targeting, School of Earth and Oceans, University of Western Australia, Crawley, WA 6009, Australia | ²School of Earth and Planetary Sciences, Curtin University, Bentley, WA 6102, Australia | ³Brunswick Exploration, Montreal, Quebec H3B 2S2, Canada | ⁴School of Earth and Atmospheric Sciences, Queensland University of Technology, Brisbane, QLD 4000, Australia

Abstract Crustal-scale transpressional shear zones provide critical insights into regional tectonics during oblique convergence and frequently host significant ore deposits. However, deciphering their evolution remains challenging due to complex interactions between orientation relative to the finite shortening, structural inheritance and strain partitioning, that influence their localisation, geometry, and kinematics. Following an integrated field-to-laboratory approach, this study investigates the record of transpressional tectonics and controls on mineralisation in the gold-endowed, north-striking Séguéla shear zone located in north-western Côte d'Ivoire, within the Paleoproterozoic Baoulé-Mossi domain, southern West African craton. The Séguéla shear zone evolved during a progressive D_{1Seg} - D_{2Seg} deformation phase associated with northwest-trending oblique convergence. D_{1Seg} likely records the Eburnean Tectonic Event (ca. 2135 to 2020-2095 Ma) culminating in craton assembly, whereas the main D_{2Seg} stage reflects late Eburnean (ca. 2095-2060 Ma) transcurrent tectonics. D_{1Seg} eastward-directed thrusting remnants persist in low-strain domains but were overprinted by high-strain, first-order north-striking shears and second-order northeast-striking structures formed during pure shear-dominated D_{2Seg} transpression. Pre-existing northeast-striking fabrics likely facilitated strain localisation, although their timing and exact role in the docking of the craton remain uncertain. Quartz microtextures indicate elevated strain intensity and/or longer-lived deformation within mineralised veins formed along first-order shear structures, contrasting with transient, possibly weaker deformation and enhanced thermal or strain relaxation recorded in second-order structures. Finally, strain partitioning across the Séguéla shear zone controls the distribution, tonnage and grade of gold deposits along first- and second-order structures, as well as ore-shoot orientation. This case study therefore highlights how integrating multiscale evidence unravels strain partitioning in transpressional systems, improving our understanding of deformation processes and their control on mineralisation.

Plain language summary Transpressional shear zones are large geological structures that form when geological blocks collide obliquely, creating zones of deformation which frequently host significant mineral deposits, including gold. Understanding how these zones form and evolve can be challenging because their history often involves multiple stages and/or phases of deformation, and interactions with older geological structures. In this study, we investigated the Séguéla shear zone, a significant gold-bearing structure in Côte d'Ivoire, within the southern West African craton. We combined field observations, drill core analysis, and microscopic investigations to reconstruct its tectonic history and control(s) on ore formation. Our results show that the shear zone records a progressive deformation history: an early stage of thrusting around 2135 to 2120-2095 million years ago, related to the assembly of the craton, followed by a later stage of transpressional strike-slip tectonics around 2095-2060 million years ago. Older northeast-striking fabrics likely guided where deformation localised, although their exact role remains uncertain. We found that mineralised quartz veins hosted in major shear structures have variable orientation along bends in strike, while preserving evidence of higher strain intensity and longer-lived deformation than veins in secondary structures, which record more transient or weaker strain. These differences in strain partitioning explain where gold deposits form, how large and rich they become, and the direction in which the richest parts of these deposits ("ore shoots") develop. The Séguéla case study therefore shows how linking observations from large-scale structures down to microscopic textures helps unravel the tectonic and mineralising history of transpressional systems.

Executive Editor:
Craig Magee
Associate Editor:
Sebastian Zapata
Technical Editor:
Roxana Stanca

Reviewers: Gerold Zeilinger Sebastian Zapata

Submitted:
21 April 2025
Accepted:
21 August 2025
Published:
20 October 2025

Introduction 1

Transpressional shear zones are fundamental markers of oblique convergence, from the lithospheric scale (Harland, 1971) up to kilometre- and metre-scale structure (e.g., Bürgmann and Pollard, 1992, 1994; Miller, 1994; Peacock and Sanderson, 1995; Westaway, 1995; Nevitt et al., 2014; Nabavi et al., 2017). These zones are also prime sites for the formation of structurally controlled ore deposits, particularly in contractional steps or restraining bends where fluid flow and strain localisation are enhanced (e.g., Miller et al., 2000; Sibson, 2001; Cox and Ruming, 2004; Tornos et al., 2005; Micklethwaite et al., 2010; Martin-Izard et al., 2016; del Real et al., 2023; Hauteville et al., 2025).

The interplay between simple shear and contraction orthogonal to the shear plane in transpressional shear zones exerts a first-order control on the localisation, geometry, and kinematics of deformation structures across multiple scales (Sanderson and Marchini, 1984; Krantz, 1995; Dewey et al., 1998; Fossen and Tikoff, 1998). However, mechanical complexity inherent to (i) transpressional shear zone development (e.g., Fossen et al., 1994; Tikoff and Teyssier, 1994; Fossen and Tikoff, 1998), and (ii) structural inheritance make the controls of strain partitioning on deformation and ore style (i.e., distribution, geometry and style) in such systems difficult to quantify. Notably, deformation is commonly accommodated heterogeneously through strain partitioning, whereby inherited, favourably oriented structures act as second-order strain-localising zones within broader, crustal-scale shear systems in mid- to lower-crustal settings (Dewey et al., 1998; Cunningham and Mann, 2007). This process adds complexity to the interpretation of protracted and/or progressive tectonic record across ductile shear zones resulting from oblique tectonics (Gremmel et al., 2024 and references therein). Understanding strain partitioning and influence of structural inheritance during transpression is therefore essential for deciphering regional tectonic evolution (Diraison et al., 1998; Fossen and Tikoff, 1998; Solar and Brown, 2001; Choulet et al., 2012; Wu et al., 2023) and linking them with ore-forming processes.

In this study, we investigate these concepts through an integrated analysis of the Paleoproterozoic, north-striking Séguéla shear zone, that remains overlooked despite its strategic location for investigating the tectonic record of the Paleoproterozoic southern West African craton (sWAC) assembly, and its significant gold endowment. The study area lies at the easternmost transition zone between the Archean Kénéma-Man nucleus and the Paleoproterozoic Baoulé-Mossi domain in Côte d'Ivoire (Figure 1a), which were docked together during northwest-trending oblique convergence at ca. 2150-2095 Ma (Caby et al., 2000; Egal et al., 2002; Feybesse et al., 2006; Eglinger et al., 2017; Wane et al., 2018; Masurel et al., 2022; Perret et al., 2025). Recent documentation by Weedon et al. (2023) identifies the Séguéla shear zone as sinistral-slip, but no attention has been brought to the restraining bend geometry of its central part, comprising north- to northeast-striking major magnetic lineaments (Figure 1b, c). This shear zone hosts several gold deposits distributed along both lineament sets, with cumulative proven and probable reserves of 1154 koz (i.e., 35.9 t Au) for the Séguéla gold project (Figure 1b, c; Weedon et al., 2023). The distribution of gold deposits along multiple sets of crustal-scale structures within the Séguéla shear zone therefore provides a compelling case to investigate the relationship between shear zone evolution in a transpressional setting and gold mineralisation.

We focus on five deposits: (i) Antenna, Ancien, and Sunbird along north-striking structures, and (ii) Koula and Boulder along northeast-striking structures (Figure 1b, c). Field observations and oriented drill core logging elucidate the geometry, texture, interconnection, and orientation of mineralised quartz veins and their relationships with structural fabrics. This approach aims to elucidate fluid-assisted deformation dynamics and fluid-rock interactions at scales ranging from the deposit to the shear zone (e.g., Beach, 1977; Robert et al., 1995; Sibson, 1996; Cox et al., 2001; Oliver and Bons, 2001; Cox, 2010; Bons et al., 2022). Additionally, microtextures of mineralised quartz veins are investigated using optical microscopy and electron backscattered diffraction (EBSD) analysis, providing insights into mechanical vein formation and post-crystallisation deformation history, and local strain partitioning (e.g., Ramsay and Huber, 1987; Drury and Urai, 1990; Urai et al., 1991; Bons and Jessell, 1997; Bons, 2000; Passchier and Trouw, 2005; Bons et al., 2012). In this study we follow the methodology of Brochard et al. (2023), built on the methodology of Cross et al. (2017) for post-processing of EBSD maps, who validated the approach for hydrothermal auriferous quartz vein.

Combining these multidisciplinary enables a comprehensive discussion of transpression and strain partitioning along the Séguéla shear zone, from the crustal to the microscale. Ultimately, we provide insights into the relationships between transpressional shear zone evolution, stress partitioning, and ore formation processes, resulting into a differential ore endowment between first- and second-order structures within the Séguéla transpressional system.

Geological setting

The southern West African craton

The sWAC represents the southern segment of the West African craton, which extends northward into northern Africa and includes the Anti-Atlas inliers (Kennedy, 1964). The sWAC comprises the Archean Kénéma-Man domain to the west (Bessoles, 1977; Boher et al., 1992) and the Paleoproterozoic Baoulé-Mossi domain to the east (Bonhomme, 1962; Bessoles, 1977) (Figure 1a). The Kénéma-Man domain consists predominantly of ca. 3500-2600 Ma Archean crust, which is well preserved

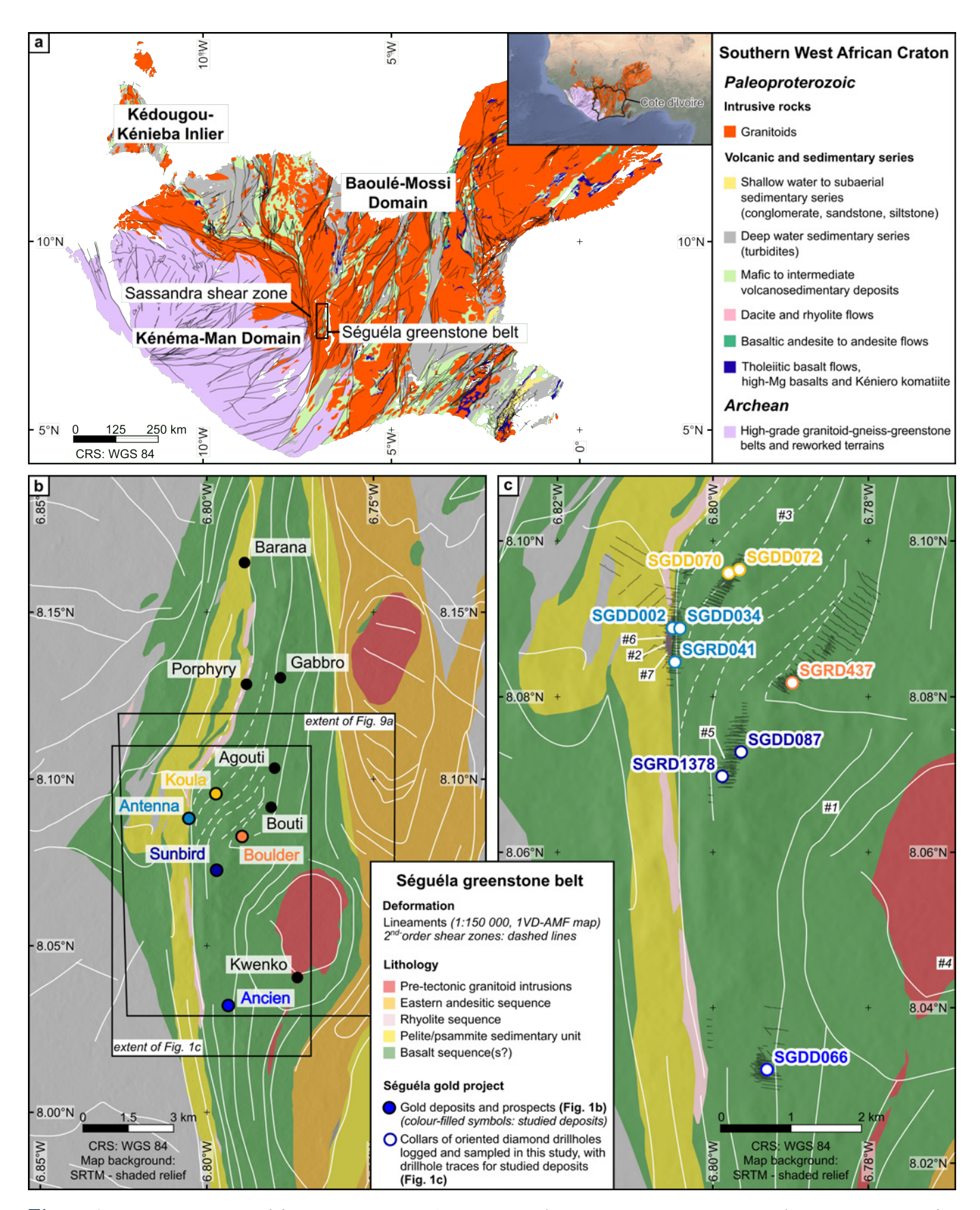


Figure 1 – Geological maps of (a) the southern West African craton (modified after Perret et al., 2025), with an inset and (b, c) the Séguéla gold project (modified after Criddle et al., 2021). Interpreted lineaments are derived from the 15 m-resolution first vertical derivative of the amplitude of the anomalous magnetic field map of the area (1VD-AMF, Supplementary File 1). Dashed lines represent second-order structures. (b) Locations of studied gold deposits and (c) positions of logged diamond drill holes. Colours selected to represent deposits are consistently used across subsequent figures to differentiate observations. Extents of Figures 1c and 9a are shown in b. Locations of photographs shown in Figures 2 and 3 (#1 to #7) are indicated in c.

in its western part but extensively reworked during the Paleoproterozoic to the east (Kouamelan et al., 1997; Eglinger et al., 2017; Koffi et al., 2022; Kouamelan et al., 2015). The Baoulé-Mossi domain formed between ca. 2350-2000 Ma during the Eburnean-Transamazonian orogeny (Grenholm, 2019 and references therein). It consists of a network of linear to arcuate greenstone belts, sedimentary basins, and plutonic domains, all transected by major regional-scale shear zones (Bessoles, 1977; Feybesse et al., 1989; Feybesse and Milési, 1994; Kouamelan et al., 1997; Caby et al., 2000; Egal et al., 2002; Baratoux et al., 2011; Perrouty et al., 2012; Grenholm et al., 2019a; Baratoux et al., 2024). A recent, comprehensive synthesis integrating lithological, geochemical, geochronological, structural, metamorphic, and metallogenic datasets suggests that the sWAC records the transition from Archean-style to modern-style plate tectonics (Perret et al., 2025).

At the crustal scale, the transition between the Kénéma-Man and Baoulé-Mossi domains is centred along the Sassandra shear zone, marking the collision of Paleoproterozoic terranes at ca. 2095 Ma (Figure 1a; e.g., Eglinger et al., 2017; Chardon et al., 2020; Traoré et al., 2022). However, U-Pb-Hf isotopic analyses of zircon indicate significant Paleoproterozoic reworking of Archean crustal components on both sides of the transition zone (pers. comm. N. Thébaud). It raises questions regarding the exact width of the transition zone, timing of its formation and/or reactivation, the position and extent of potentially deeply rooted inherited structures, and their lithospheric-scale implications (e.g., Feybesse et al., 1989; Feybesse and Milési, 1994).

2.2 The Séguéla greenstone belt

The north-striking Séguéla greenstone belt is located at the easternmost boundary between the Archean Kénéma-Man and the Paleoproterozoic Baoulé-Mossi domains in Côte d'Ivoire (Figure 1a). The belt is approximately 100 kilometres in length, with a maximum width of 5-10 kilometres, narrowing towards both north and south (Figure 1a, b).

Stratigraphic record 2.2.1

Despite recent lithological and geochemical investigations within the Séguéla greenstone belt (Amoih, 2022; Allialy et al., 2023; Ephrem et al., 2023), detailed stratigraphic information remains sparse compared to other greenstone belts in Côte d'Ivoire (e.g., Mériaud et al., 2020; Hayman et al., 2023). The stratigraphy comprises, from west to east, a sequence of basaltic flows interlayered with fine-grained siliciclastic units (potentially volcano-sedimentary; Amoih, 2022), rhyolitic flows, and a less abundant andesitic succession, all intruded by granitoid bodies (Figure 1b; Criddle et al., 2021; Amoih, 2022). A single U-Pb zircon age of 2169 ± 11 Ma for a rhyolite flow (unknown source, cited in Criddle et al., 2021) indicates that parts, if not all, of the exposed stratigraphy are coeval with the Eoeburnean (2200-2135 Ma) juvenile, calc-alkaline, bimodal volcanic

activity and associated crustal thickening documented across the central and eastern Baoulé-Mossi domain (Weedon et al., 2023; Perret et al., 2025). All facing indicators show eastward younging, and there is no evidence for major repetition of the sequence. The sequence underwent greenschist facies metamorphism (Criddle et al., 2021; Weedon et al., 2023), but there are no constraints on timing and pressure-temperature conditions reached to date.

2.2.2Tectonic framework of the Archean-Paleoproterozoic transition

Despite its key tectonic position, the structural framework of the Séguéla greenstone belt remains poorly characterised. Existing information predominantly derives from studies in adjacent regions, compiled by Grenholm et al. (2019b), including the Odienné area to the north-northwest (Caby et al., 2000), the Toulépleu-Ity domain to the southwest (Feybesse et al., 1990), the Sassandra shear zone to the west (Feybesse and Milési, 1994), and the Ferkéssédougou area to the southeast (Ouattara, 1998). earliest recognised regional-scale deformation involves west-southwest-directed thrusting and associated folding west of the Séguéla belt, resulting from late Eoeburnean to early Eburnean convergence around 2150-2100 Ma (Feybesse et al., 1990; Feybesse and Milési, 1994). Northwest-trending oblique convergence persisted until 2095 Ma, coinciding with docking of the Baoulé-Mossi and Kénéma-Man domains and sinistral strike-slip reactivation of major shear zones across the central and western Baoulé-Mossi domain (Caby et al., 2000; Egal et al., 2002; Feybesse et al., 2006; Eglinger et al., 2017; Wane et al., 2018). Subsequently, late collisional, block west-to-the-south, sinistral-slip shearing occurred along the Sassandra shear zone between ca. 2095-2060 Ma (Masurel et al., 2022; Perret et al., 2025 and references therein), consistent with deformation patterns documented in regions adjacent to the Séguéla greenstone belt (Feybesse et al., 1990; Feybesse and Milési, 1994; Ouattara, 1998; Caby et al., 2000).

2.3The Séguéla gold project

Structural record of the Séguéla gold project, central Séguéla greenstone

The emplacement of the Séguéla bimodal volcanic pile likely occurred during an early, cryptic D_{0Seg} extensional event, inferred from stratigraphic and geochemical evidence. Subsequently, two deformation stages have been identified at both belt and project scales (Criddle et al., 2021; Weedon et al., 2023):

(i) D_{1Seg} is poorly defined, represented by cryptic remnants of planar fabrics with a steeply plunging stretching lineation, formed by northwest-directed thrusting, later reoriented during subsequent non-coaxial D_{2Seg} deformation.

deformation produced the dominant penetrative fabric defining the structural framework at both belt and project scales. This fabric is a subvertical, north- to northeast-striking C/S₂ shear band cleavage (simplified as S₂ herein) formed during block west-to-the-south, sinistral-slip shearing. Deformation is primarily accommodated by high-strain shear corridors, ranging from tens to hundreds of metres in width, hosting gold deposits emplaced during the D_{2Seg} deformation stage.

The main penetrative fabric and shear corridors are clearly defined by lineaments interpreted from the first vertical derivative of the amplitude of the anomalous magnetic field map at a 1:150,000 scale (Figure 1b, c; Supplementary File 1). Two main lineament sets are identified. The first comprises north-striking lineaments that are parallel to the D_{2Seg} -related strike-slip shear They form the regional structural grain and define the extent of the Séguéla shear zone. The second set consists of north-northeast- to northeast-trending lineaments that are prominent within the widest central part of the belt, which is bounded east and west by major north-striking corridors (Figure 1c). These shorter lineaments tend to curve around pre-kinematic granitoid bodies, producing sigmoidal patterns indicative of apparent block west-to-the-south sinistral displacement.

Lithological, structural and 2.3.2metallogenic characteristics of the studied deposits

Information summarised below is sourced from Criddle et al. (2021) and Weedon et al. (2023). Panels b and c in Figure 1 illustrate the location of deposits studied, superimposed on a project-scale geological map for reference.

The Antenna deposit occurs along a north-striking sheared contact between a rhyolitic unit (up to ca. 150 m thick), interlayered with felsic volcaniclastics (up to 10 m thick) and a basaltic unit to the east. Gold mineralisation comprises a brittle-ductile quartz-albite vein stockwork, predominantly within the flow-banded rhyolitic unit, near their sheared contact with basalts to the east. Hydrothermal mineralisation is associated with pyrite and pyrrhotite, and follows a progressive alteration pattern, i.e., proximal quartz-albite-(biotite-chlorite), intense intermediate quartz-albite-sericite-(chlorite), distal sericite-carbonate assemblages.

The Ancien deposit is hosted entirely within the basalts along a major north-striking shear zone. hydrothermal gold mineralisation is structurally controlled by brittle-ductile shearing and quartz-carbonate veining, associated primarily with pyrite and minor pyrrhotite. The alteration assemblage comprises biotite, sericite, and quartz.

The Sunbird deposit shares a similar lithological setting to Ancien, although it contains sparse felsic and dioritic intrusions. It is also controlled by a subvertical, north-striking shear zone. Hydrothermal

mineralisation mainly occurs within basalts, with minor mineralised lenses in rhyolitic and dioritic intrusions. The mineralised zones are characterised by intense shearing with biotite-sericite-(quartz) alteration and pervasive quartz-(carbonate) veining.

The Koula deposit, located within the same basaltic unit as Ancien and Sunbird, is controlled by a $northeast-striking \quad shear \quad corridor \quad approximately \quad 15$ metres wide, which merges with north-striking shear corridors controlling these other deposits. Hydrothermal mineralisation occurs within strongly sheared zones featuring biotite-sericite-(quartz) alteration quartz-carbonate veins.

The Boulder deposit is hosted within the same basaltic unit, with presence of pre-tectonic, quartz-feldspar-biotite porphyritic felsic intrusions and a gabbro unit in its western part. The deposit is controlled by a north-northeast-striking shear zone, with hydrothermal gold mineralisation occurring as quartz-(carbonate) veins associated with pyrite and pyrrhotite, hosted in schistose to mylonitic basalt and along felsic intrusion margins.

Field data collection and analytical methods

Fieldwork and sampling approach

Field investigations were conducted across the Séguéla gold project area, with lithological and structural observations collected using the GEOL-QMAPS digital geological mapping solution (Perret et al., 2024; Perret, 2025). Descriptions of mineralised features were limited to Antenna, the only open pit existing at the time of fieldwork. All field observations and measurements are provided in Supplementary File 2.

In addition, a selection of oriented diamond drill cores from deposits located along first-order (Antenna, Ancien, and Sunbird) and second-order (Koula and Boulder) structures was logged and sampled to characterise the relationships between host rock facies, macrostructures, and mineralised quartz veins. Particular attention was given to the geometry, texture, and mineral paragenesis of mineralised veins, as well as their angles relative to the penetrative shear band cleavage. Drill hole collar locations are indicated in Figure 1c. Wherever possible, orientations of the main penetrative cleavage, stretching lineations and mineralised veins were systematically measured along drill cores using a core reorientation tool (i.e., rocket launcher) and downhole survey data provided by Fortuna Silver, to supplement existing data collected from outcrops.

Analytical methods 3.2

3.2.1Textural and paragenetic description of mineralised veins, quartz microtextures and nomenclatures

Drill cores were first described macroscopically to document lithological, structural, and mineralised

features. Although early, carbonate-dominated veins folded, transposed and dismembered along the main penetrative fabric have locally been observed on drill cores, we only focus on mineralised veins in this study.

Based on their orientation and textures, mineralised veins were classified into three categories: shear veins, extensional veins, and hybrid shear-extensional veins $(Bons\ et\ al.,\ 2012).$ Definitions and criteria for classification are as follows:

- (i) Shear veins form in response to shear displacement along pre-existing or newly formed fractures. These veins are typically oblique to the maximum principal stress and often subparallel to the shear-zone schistosity, reflecting alignment with the principal stress direction. They exhibit a mixed brittle-ductile deformation style and evidence of shear movement, such as slickensides, sigmoidal shapes, or asymmetrical fibres. Textures indicating incremental deposition are common, with the opening direction forming a very small angle with the vein (e.g., Ramsay and Huber, 1987; Passchier and Trouw, 2005).
- (ii) Extensional veins form perpendicular to the minimum principal stress, typically under conditions of fluid overpressure and tensile stress. These conditions arise when fluid pressure approaches lithostatic pressure under relatively low differential stresses (e.g., Sibson, 1981; Etheridge, 1983; Cox et al., 1991). Textures often indicate incremental cracking and mineral precipitation, suggesting episodic fluid flow and stress changes (e.g., Sibson, 1990, 1992).
- (iii) Hybrid shear-extensional veins represent transitional type influenced by both shear and extensional stresses. These veins form in environments where stress conditions fluctuate, such as during seismic cycles. Their orientations are variable and often exhibit crosscutting relationships with other vein sets and the main shear cleavage, reflecting shifts in stress orientations (e.g., Cerchiari et al., 2020).

Note that the differences in textures, orientations and formation mechanisms for shear, shear-extensional and extensional veins are widely illustrated in literature (e.g., Hodgson, 1989; Robert et al., 1995; Dubé and Gosselin, 2007; Jébrak and Marcoux, 2008; Bons et al., 2012; Miller, 2014; Sibson, 2020).

Microscopic petrography was performed on oriented thin sections prepared from samples collected along oriented diamond drill cores. Transmitted light microscopy images in plane-polarised light (PPL) and cross-polarised light (XPL), as well as reflected light (RL) images, were acquired using a Zeiss Axio Imager microscope located in the School of Earth and Planetary Sciences at Curtin University, Perth, Australia. Petrographic and microstructural analyses focused on identifying the mineral assemblages associated with gold mineralisation and characterising microtextures. Special emphasis was placed on dynamic

and static recrystallisation patterns in mineralised quartz veins to identify regions of interest for further EBSD analysis.

3.2.2Electron back-scattered diffraction analysis of mineralised veins

EBSD analyses were conducted to investigate the dynamic and static recrystallisation of mineralised quartz veins. Four samples were selected to represent the variability in quartz grain size distribution and recrystallisation patterns between shear and extensional veins, as well as across deposits associated with firstand second-order structures at the scale of the Séguéla gold project (Figure 1c; Table 1). EBSD analyses were conducted at the John de Laeter Centre, Curtin University, Perth, Australia, to investigate the dynamic and static recrystallisation of mineralised quartz veins. Analyses were performed on a Tescan Mira3 field emission gun scanning electron microscope, equipped with an Oxford Symmetry EBSD detector, at a 20 kV accelerating voltage in "large-area" map mode. The working distance was fixed at 20 mm. fields were processed and stitched together using the Oxford Aztec Crystal software. Each map (n = 4)utilised approximately 10 hours of instrument time. The samples analysed in this study displayed varying textures and grain sizes. Consequently, the step size for EBSD mapping was adjusted according to the minimum recrystallised grain size in each sample (i.e., 2.2 to 9.8) micrometres; Table 1).

The EBSD orientation maps of quartz obtained were of good quality: the indexing rate for EBSD analyses ranged from 53% to 83% across all samples (Table 1). This rate could have been improved if secondary phases were included in the analysis, such as calcite, biotite, pyrite and white mica (see section 4.2). Photographs of the core samples with location of the thin sections, scans of the thin sections prepared, raw Aztec EBSD images are available as Supplementary File 3. It also contains EBSD post-processed data (see section 3.2.3) such as MatLab figure files and spreadsheets.

3.2.3 Separation of relict and recrystallised grains

Post-processing of EBSD maps was performed using the MTEX MATLAB toolbox (Bachmann et al., 2010, 2011; https://mtex-toolbox.github.io/) and the code developed by Brochard et al. (2023), adapted from Cross et al. (2017). The primary objective of the analysis was to distinguish between relict and recrystallised grains, and evaluate the grain size distribution of recrystallised grains. The workflow consisted of the following steps:

- (i) EBSD data were loaded, and individual quartz grains were identified using a 10° misorientation threshold to define grain boundaries (White and White, 1981; Shigematsu et al., 2006),
- (ii) Wild spikes in the EBSD data, corresponding to single-pixel grains, were removed to improve computational efficiency,

- (iii) Quartz grains separated by boundaries with $60 \pm 5^{\circ}$ rotations around the c-axis were merged, as these correspond to single grains containing Dauphiné twins,
- (iv) Poorly constrained grains were excluded using a minimum threshold for the fraction of each grain's area composed of indexed pixels, as outlined by Cross et al. (2015). Grains composed of fewer than four pixels were also discarded, as these may result from misindexing. The minimum threshold was lowered for sample SG41-03 to better separate relict and recrystallised grains, because of the larger grain size and lower spatial resolution (9.8 micrometres; Table 1),
- (v) Intragranular deformation within individual grains was quantified by calculating the misorientation between each pixel and the grain's mean orientation. Relict grains, characterised by relatively high intragranular lattice distortion, were distinguished from recrystallised grains, which exhibit low intragranular distortion. This classification was achieved by applying a grain orientation spread threshold (Wright et al., 2011),
- (vi) Grains intersecting the edges of the EBSD map were removed before conducting grain size analyses. The area-equivalent circle diameters were then calculated for both relict and recrystallised grains,
- (vii) All samples displayed unimodal grain size distributions, eliminating the need to consider multiple populations for grain size calculations. Grain size statistics and distributions exported.

further details on the limitations For recommendations for applying this methodology, refer to Cross et al. (2017); Brochard (2022); Brochard et al. (2023). Details about calculation of standard deviation for grain size conducted in this study are documented in *Brochard et al.* (2023).

Several additional key limitations must be considered when interpreting the results. The followed approach assumes that dislocation density can be used to differentiate relict from recrystallised grains. However, (i) at higher temperatures, dislocations do not accumulate significantly, as syn-deformational recovery equilibrates the system, and (ii) at lower temperatures, newly nucleated grains (e.g., from bulge recrystallisation) may initially retain very low dislocation densities, expanding outward and consuming older, deformed grains. While these grains are technically recrystallised, they will develop internal deformation structures over time. These factors illustrate that natural deformation processes are far more dynamic than the simplified model of dislocation density-based grain classification allows, and that a thorough optical microscopy study of microtextures is required prior to interpreting such results.

Results

Lithological and structural framework of the central Séguéla greenstone belt

4.1.1 Lithological framework

Basaltic flows interlayered with minor fine-grained (volcano)-sedimentary intervals, rhyolitic flows, and pre-kinematic granitoid intrusions are exposed in the studied area (Figures 1c, 2). Observing primary volcanic and sedimentary textures is challenging due to pervasive structural overprinting and hydrothermal alteration which manifests through variable assemblages of quartz-albite-biotite-sericite-chlorite-ankerite within D_{2Seg} -related mineralised shear corridors (Weedon et al., 2023). Nonetheless, weakly deformed and altered basalt exposures displaying pillow lava structures are observed in lower-strain areas between shear corridors (Figure 1a). Pillow asymmetry and S_0 pillow bedding orientations (e.g., N310°-52°, another N356°-50° measurement east to Agouti deposit; Figure 1c) indicate an eastward-facing direction.

Fine-grained siliciclastic volcano-sediments rhyolitic flows occur predominantly along the western margin of the Séguéla shear zone (Figure 1c). Volcano-sediments typically comprise volcanic quartz and silt-sized components. They are overall highly sericite-rich and exhibit a pronounced schistosity (Figure 2b). In contrast, rhyolitic flows are less deformed but feature sheared contacts subparallel to the S_2 penetrative fabric which is particularly evident in the strongly schistose basalt unit (Figure 2c).

The major intrusive granitoid is the K-rich Kwenko granite pluton, located in the eastern part of the belt (Figures 1c, 2d). Its pre-kinematic emplacement is evidenced by an oblate, slightly sigmoidal geometry with its margins wrapped by magnetic lineaments indicative of shear strain (Figure 1c). The pluton displays a S₂ tectonic foliation preferentially developed near its contacts with the surrounding basalts (Figure 2d).

4.1.2 Structural framework

The structural framework of the central Séguéla greenstone belt is dominated by a north-striking shear zone, up to 10 kilometres in width, comprising two sets of high-strain shear corridors. These shear corridors, up to hundred metres in width, strike northwards or north-northeast- to northeastwards, as identified in aeromagnetic dataset (Figure 1b,c; Criddle et al., 2021). Outside these high-strain corridors, rare evidence of an earlier ductile D_{1Seg} deformation stage is preserved as north-striking, gently east-dipping, C₁ thrusts that are tens of metres in width and transect pillow basalts (e.g., C₁ thrust oriented N004°-34°E in Figure 3a). Distortion of the basalts indicates apparent top east-to-the-west thrust kinematics (Figure 3a). Yet, the absence of stretching lineation and kinematic indicators precludes the interpretation of the true displacement direction and the estimation of the throw. Documenting these features

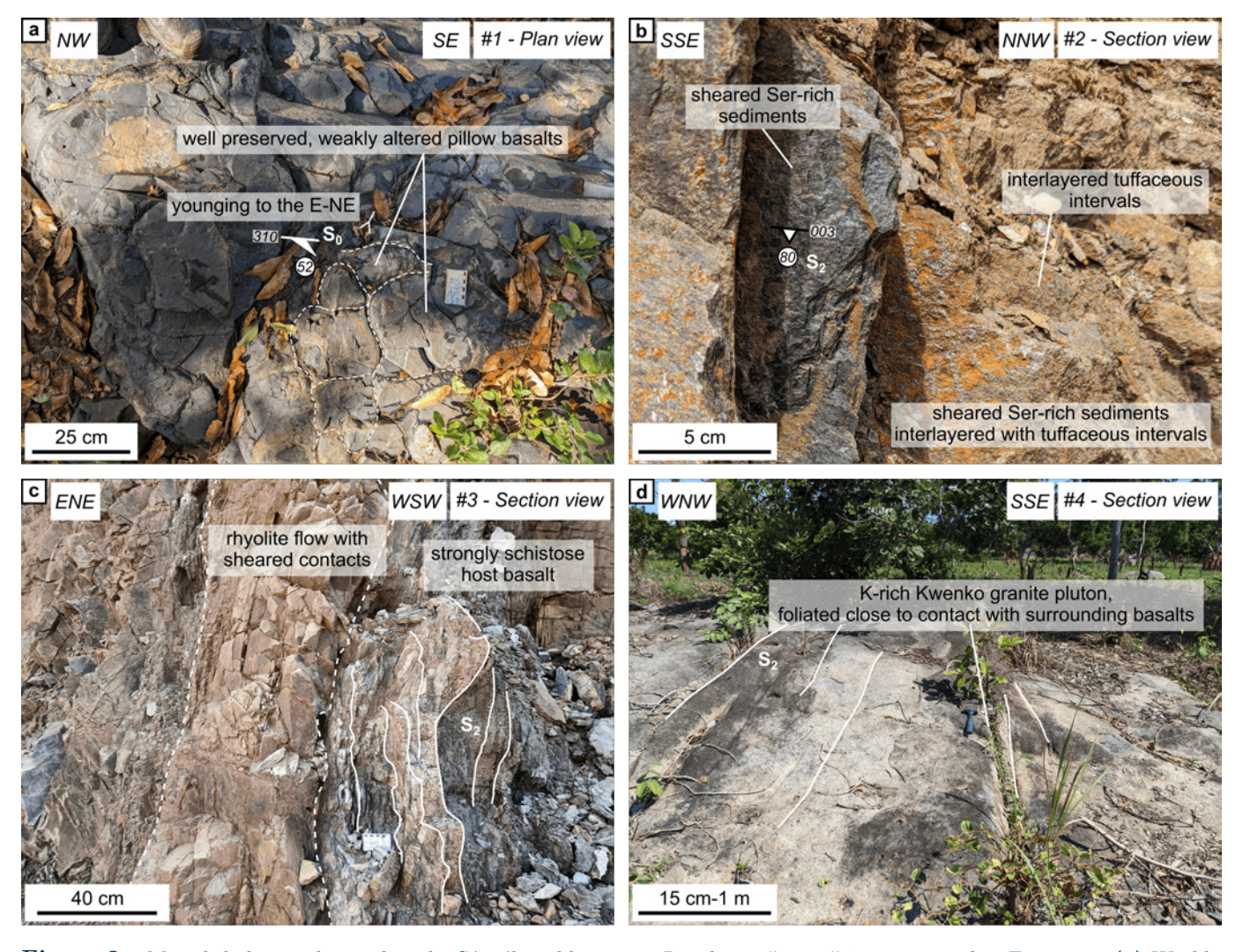


Figure 2 – Main lithologies observed in the Séguéla gold project. Localities #1 to #4 are reported in Figure 1c. (a) Weakly deformed and altered pillow basalts showing an eastward facing direction. (b) Sericite (Ser)-rich psammitic to pelitic sediments interlayered with felsic tuffs, strongly schistose, and recording dominant S₂ shear band cleavage. (c) Rhyolitic flows interlayered with basalts and volcano-sediments; contacts sheared along the S₂ fabric. (d) Pre-tectonic Kwenko granite, exhibiting a marginal S_2 tectonic foliation indicated by parallel fractures.

is further complicated by their rarity in outcrop across the Séguéla shear zone and the limited availability of oriented diamond drill holes, which primarily target the D_{2Seg}-related, gold-endowed, high-strain shear corridors (Figure 1c).

The ductile-(brittle) D_{2Seg} deformation is partitioned into subvertical, northeast- to north-striking, high-strain C_2 shear corridors (Figures 1c, 3b-d). These structures strongly overprint primary textures and earlier fabrics. Two distinct sets of C₂ shear corridors match interpreted magnetic lineament sets (Figure 1b): north-striking corridors and second-order northeastto north-northeast-striking corridors, also observed on outcrops (Figure 3b, c) and oriented diamond drill cores (Figure 3d, e).

First-order shear corridors strike consistently northward and display subvertical S₂ shear band In details, its strike varies slightly from $N000^{\circ}-N175^{\circ}$ at Sunbird to $N005^{\circ}-N010^{\circ}$ at Antenna and Ancien (Figure 4a). A prominent shallowly northor south-plunging L₂ stretching lineation, primarily

defined by sericite and chlorite, is recorded along the S_2 fabric (Figure 3b-d). It is well developed at Sunbird compared to Antenna and Ancien (Figure 4a). Kinematic indicators, including slickensides (Figure 3b, d) and asymmetric quartz tension gashes (Figure 3c), demonstrate a block west-to-the-south sinistral-slip motion (Figure 4a). The main fabric weakens and deflects outside these corridors, possibly reflecting pre-existing fabric preservation, local C-S fabric development, or interactions with second-order shear corridors (e.g., Antenna and Ancien; Figure 4a).

Second-order shear corridors are also subvertical but display greater variability in strike direction (N010°-N045°), influenced by proximity to bounding first-order shear zones (Figures 1b, 4b). stretching lineations in second-order corridors are sparse, predominantly dip-plunging, weakly developed, and lack clear kinematic indicators except for stepped S₂ cleavage patterns tentatively suggesting block west-down kinematics at Koula (Figure 3e; 4b).

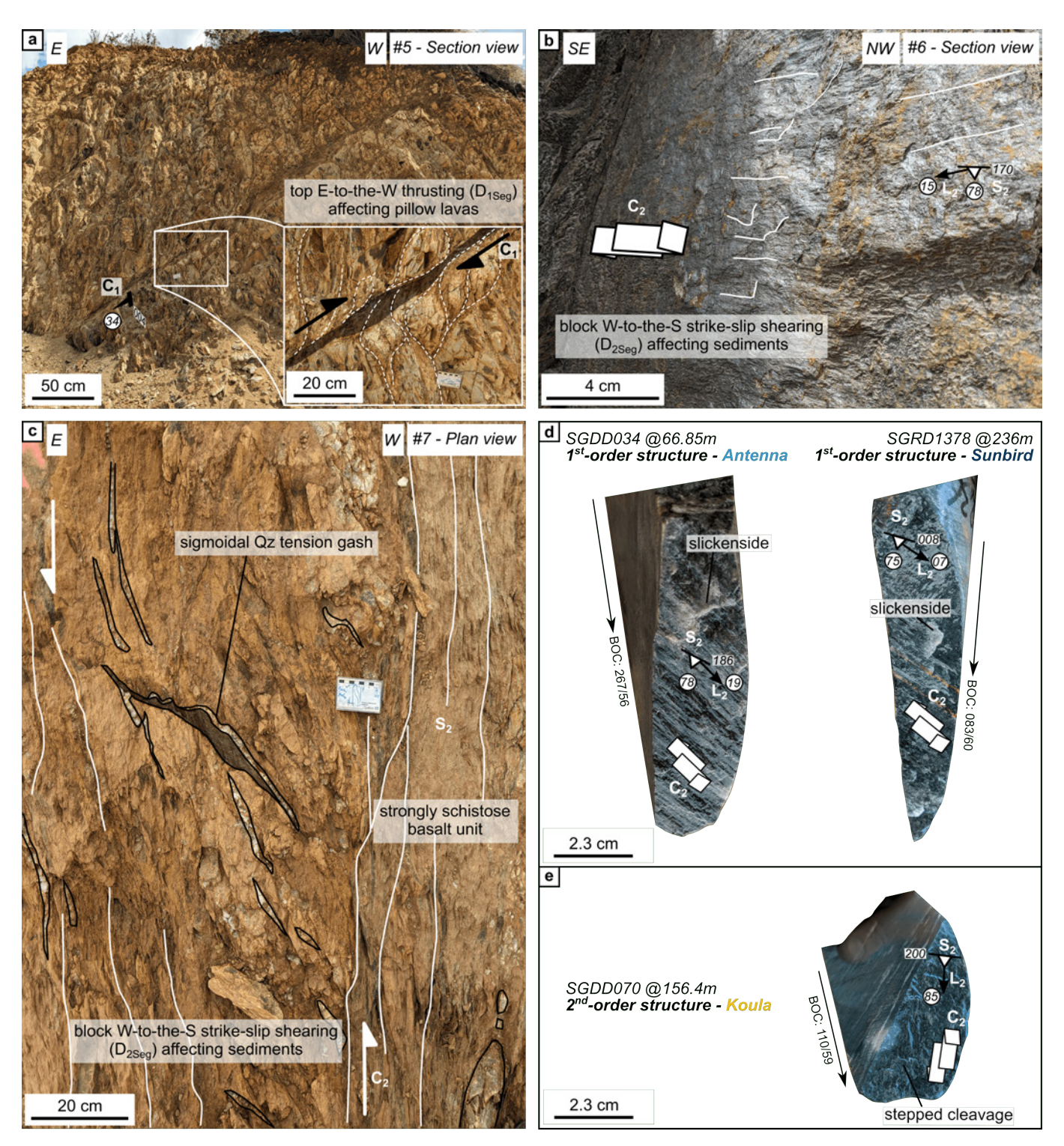


Figure 3 – Main structural features observed in the Séguéla gold project. Localities #5 to #7 and collars of drill holes are reported in Figure 1c. (a) East-dipping, top east-to-the-west thrust affecting pillow basalts, representing early D_{1Seg} deformation preserved away from C_2 shear corridors. (b) Subvertical, north-striking S_2 cleavage in schistose sediments containing a L_2 stretching lineation marked by sericite, with steps and slickensides showing block west-to-the-south, sinistral-slip kinematics. (c) Asymmetric quartz tension gashes confirming block west-to-the-south sinistral-slip motion along first-order shear corridors. (d) Slickensides along north-striking first-order shear structures indicating block west-to-the-south, sinistral-slip kinematics. (e) Second-order shear structures strike north-northeastwards, and rare stepped cleavage suggests block west-down kinematics. BOC stands for bottom-of-core orientation line.

4.2 Mineral paragenesis, orientation and quartz microtextures of veins

4.2.1 Vein types and mineral paragenesis

Gold deposits within the Séguéla project primarily occur along high-strain, first- and second-order C₂ shear

corridors (Figure 1b). They commonly develop at lithological interfaces separating units with contrasted rheological characteristics. This is particularly evident at the Antenna deposit located along the interface between a thick rhyolitic unit and the basalt sequence (see section 2.3.2).

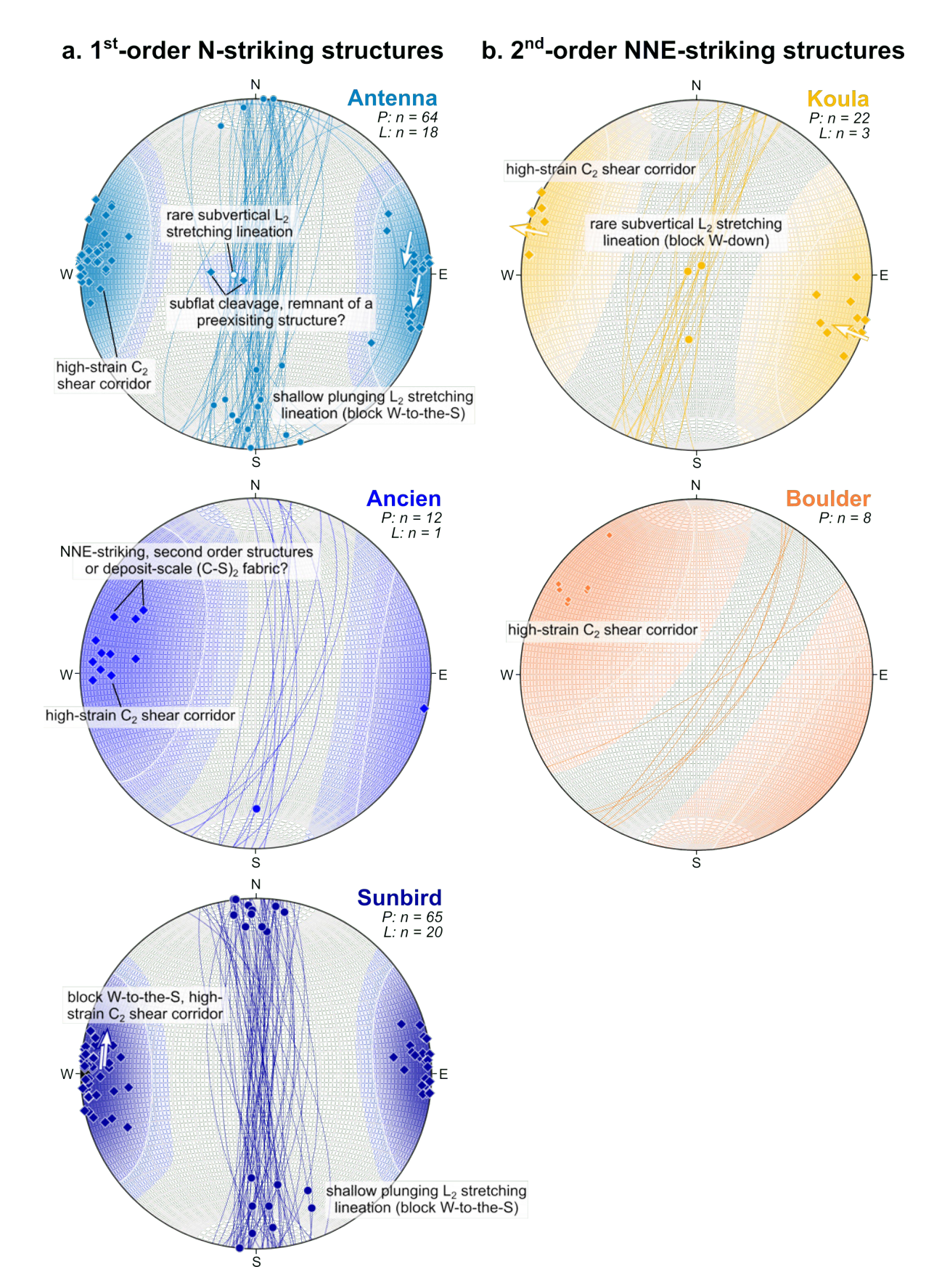


Figure 4 - Orientation of the S₂ penetrative shear band cleavage across the Séguéla gold project, along (a) first-order and (b) second-order C₂ shear corridors. Measured planes (great circles), poles to planes (diamonds), and L₂ stretching lineations (circles) are displayed on an equal-area, lower hemisphere stereonet. The number of planar and linear measurements is indicated for each deposit. For S2 planes with resolved kinematics, hangingwall displacement is denoted by an arrow on the pole-to-plane symbol. Kamb contours of the penetrative fabric poles are shown at 1σ intervals, with the 3σ significance level highlighted in white (Kamb, 1959).

At the deposit scale, the rheology of host rocks strongly influences the localisation of mineralised veins. Competent units, such as rhyolite or felsic sediments, host both shear and extensional veins (Figure 5a), whereas more schistose units, such as strongly sheared basalt, predominantly contain shear veins (Figure 5b). Shear veins locally infill the S_2 shear band cleavage by feeding from extensional veins (Figure 5c). In the most schistose units, shear veins are typically thinner, often buckled, sometimes dismembered, and strongly stacked along the S₂ fabric. Rare extensional veins in these units appear folded, sheared and transposed along the S₂ penetrative cleavage (Figure 5a, b). Regardless of their orientation, the mineral assemblage and associated proximal alteration in deformed veins remain consistent with those in undeformed mineralised veins.

Mineralised veins are primarily composed of quartz with minor calcite, biotite, sericite, pyrrhotite, and/or pyrite, and with visible gold (Figure 5d-f). mineral assemblage is consistent across extensional, shear-extensional, and shear veins. Proximal alteration halos characterised by albite-sericite-(carbonate-pyrite) preferentially extend along the S_2 penetrative cleavage (Figure 5c, e, f). Pyrrhotite dominates over pyrite within mineralised veins as millimetric grains or aggregates (Figure 5e), whereas pyrite, more abundant within proximal alteration halos, occurs as isolated, undeformed grains or stringers aligned with the S_2 fabric (Figure 5f). Shear veins occasionally include host-rock fragments that delineate the S_2 shear band cleavage (Figure 5e).

4.2.2 Vein orientation

Shear veins dominate across studied deposits, though shear-extensional and extensional veins occur more frequently along second-order north-northeast-striking shear corridors (Figure 6). Shear veins align with the steep, north- to north-northeast-striking S_2 cleavage within first-order shear zones (Figure 6a) and northeast-striking S₂ cleavage in second-order shear corridors (Figure 6b).

The orientation of extensional veins within deposits along first-order shear zones reveals two scenarios (Figure 6a). At Antenna, shear, shear-extensional, and extensional veins share a common strike but show progressively shallower dips from subvertical shear to flat extensional veins. At Ancien, despite a lack of extensional vein measurements, a similar trend from shear to shear-extensional veins implies In contrast, extensional comparable relationships. veins at Sunbird strike east-northeast and dip steeply north-northwest, differing notably from Antenna and Ancien vein orientations. Nevertheless, extensional veins at all deposits display consistent textures, mineral assemblages, and crosscutting relations with structural features.

4.2.3 Quartz microtextures

Quartz-dominated, mineralised veins were classified based on their location (i.e., along first- or second-order shears) and type (i.e., extensional or shear vein) to describe quartz microtextures. These descriptions consider relict grain deformation, subgrain and recrystallised grain size and shape, and dominant recrystallisation patterns observed, following the approach of Brochard et al. (2023). Note that quartz recrystallisation textures consistently overprint primary vein textures, indicating it reflects deformation postdating vein crystallisation.

Extensional veins within first-order corridors contain irregularly shaped, millimetre-scale porphyroclasts, exhibiting patchy to undulose extinction (Figure 7a, b). These porphyroclasts display bulging boundaries, particularly evident in Figure 7a, with bulges typically less than 50 micrometres in Dynamically recrystallised grains are sparsely distributed at rims and locally form core-and-mantle structures around porphyroclasts (Figure 7a; Passchier and Trouw, 2005). Recrystallised grains occupy a low proportion of the vein volume regarding porphyroclasts. The dominant recrystallisation mechanism in these veins is therefore bulging. In Figure 7b, however, subgrains predominate and the main recrystallisation process expressed is likely subgrain rotation, despite relict grains and subgrains are not particularly elongate.

Shear veins along first-order shear zones are characterised by elongate relict grains aligned along the S_2 shear band cleavage, up to 1 millimetre in length, with undulose extinction, and recrystallised grains ranging from less than 10 to over 100 micrometres in size (Figure 7c, d). Unlike extensional veins, the difference in grain size between relict grains and recrystallised grains is less pronounced and recrystallised grains form a larger proportion of the vein volume. Two main recrystallisation mechanisms are observed: (i) subgrain rotation, where flattened relict grains transition into subgrains and recrystallised grains with weakly developed preferred orientations, and (ii) grain boundary migration, which produces recrystallised grains with interlobate boundaries resembling adjacent relict grains.

In second-order shear corridors, extensional veins are rare, and shear veins dominate in the studied deposits. However, the quartz microtextures in these shear veins differ significantly from those in first-order structures (Figure 7e, f). The microtextures are characterised by strain-free, recrystallised grains with a uniform grain size distribution centred around 100 micrometres. These grains exhibit straight boundaries and 120° triple junctions, with little to no evidence of intracrystalline deformation. These microtextures are attributed to static recrystallisation, specifically grain boundary area reduction, which overprinted pre-existing dynamic recrystallisation textures after deformation ceased.

Recrystallised grain size distribution in quartz veins

Four EBSD maps were acquired from mineralised extensional and shear veins located along the and firstsecond-order Séguéla shear corridors.

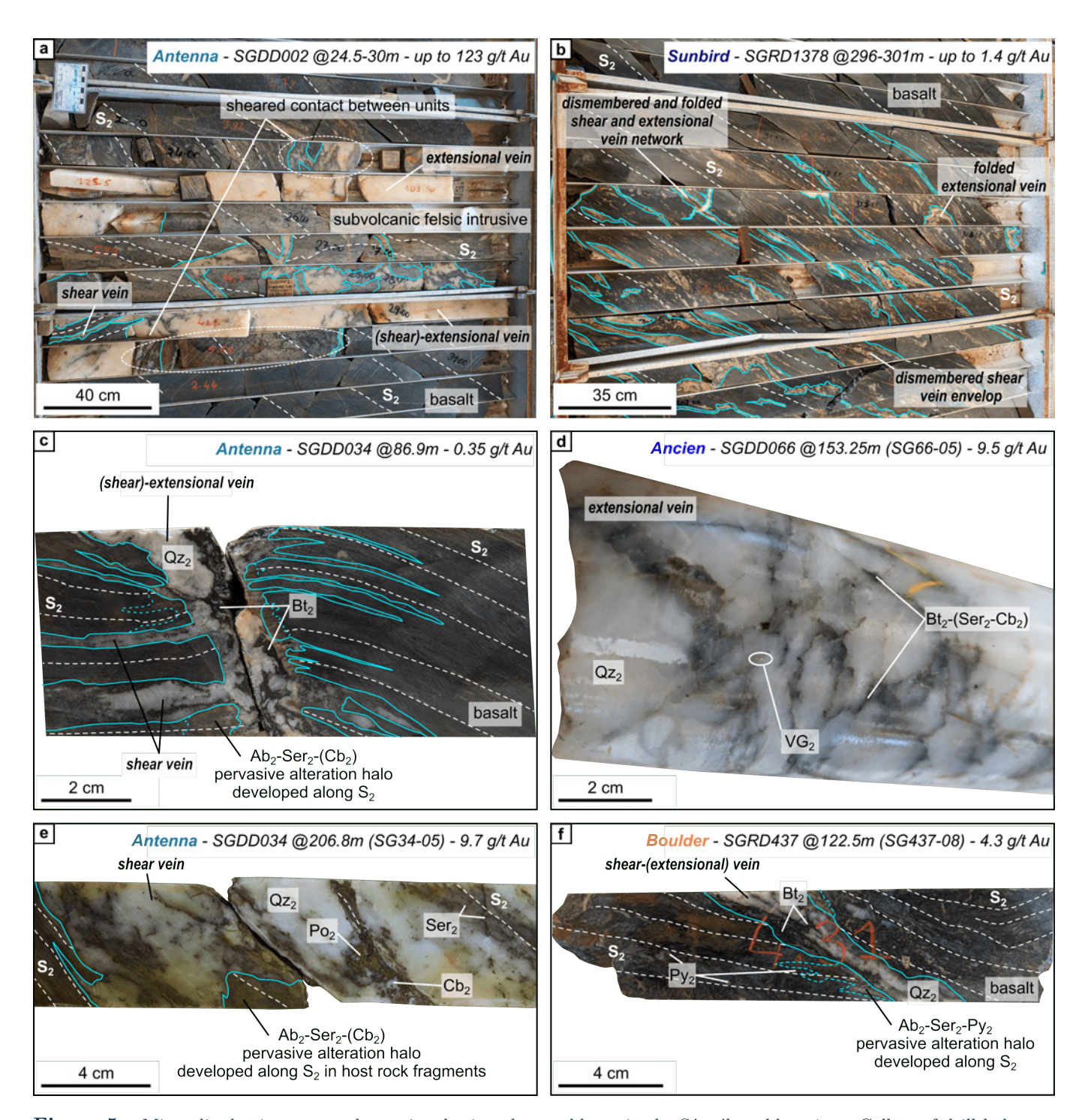


Figure 5 - Mineralised vein types and associated mineral assemblages in the Séguéla gold project. Collars of drill holes are reported in Figure 1c. Vein envelops and proximal alteration halo are in light blue, plain and dashed contours, respectively. (a) Quartz-carbonate extensional and shear veins synchronous with S₂ cleavage formation at sheared lithological contacts (e.g., basalt and felsic intrusions with contrasting rheology). (b) Stacked, buckled to dismembered shear veins aligned along S₂ fabric with folded to transposed extensional veins. Sericite-carbonate-pyrite proximal alteration follows the S_2 fabric. (c) Shear veins infilling S₂ cleavage from quartz (Qz)-biotite (Bt) extensional veins; albite Ab)-sericite (Ser)-carbonate (Cb) alteration propagates along the shear fabric. (d) Mineralised quartz (Qz) extensional vein containing sericite (Ser), carbonate (Cb), and visible gold (VG). (e) Quartz (Qz) shear vein containing pyrrhotite (Po) aggregates, altered host-rock fragments, and sericite (Ser) inclusions aligned with S₂ cleavage. (f) Isolated, millimetric pyrite (Py) grains and stringers disseminated along the S₂ fabric, proximal to quartz (Qz)-biotite (Bt) shear veins.

Post-processing enabled mapping the distribution of relict vs recrystallised grains, plotting grain size distributions (Figure 8), and calculation of the geometric mean and standard deviation of recrystallised grain sizes (Table 1).

The extensional vein sample SG41-03 from drill hole SGRD041 at the Antenna deposit (first-order structure; Figure 1b, c) exhibits features of bulge dynamic recrystallisation, with millimetric to centimetric relict grains showing undulose extinction (Figure Approximately one-third of mapped grains

a. 1st-order N-striking structures b. 2nd-order NNE-striking structures Ν **Antenna** Koula n = 21n = 1shear veins shear-extensional veins shear vein -E ·E W extensional veins shear veins Ś Ν **Ancien Boulder** n = 8 shear veins shear-extensional veins - E ·E W shear veins Ś Ś Ν **Sunbird** shear veins shear yeins shear-extensional veir

Figure 6 – Orientation of shear, shear-extensional and extensional mineralised veins at studied deposits along (a) first-order and (b) second-order C₂ shear corridors. Measured vein planes (great circles) and poles to vein planes (triangles) are displayed on an equal-area, lower hemisphere stereonet. The number of vein measurements is indicated for each deposit.

extensional veins

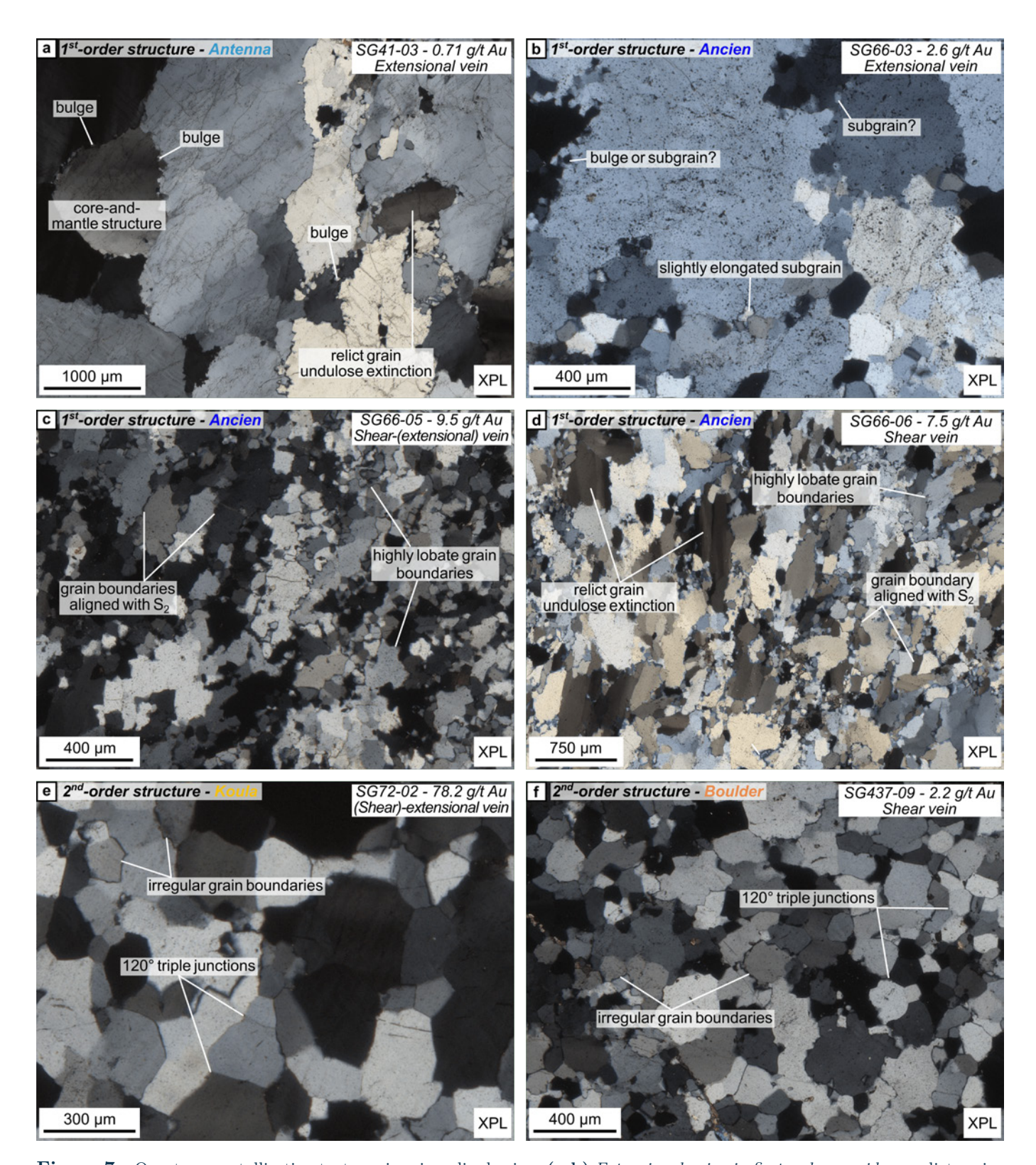


Figure 7 – Quartz recrystallisation textures in mineralised veins. (a-b) Extensional veins in first-order corridors: relict grains remain coarse (exceeding 1 millimetre in size) and exhibit undulose extinction, recrystallisation of bulges, and core-and-mantle structures in extensional veins, as well as some subgrains locally elongate. (c-d) Shear veins in first-order corridors: subgrain rotation (elongate grains aligned with S₂) and grain boundary migration (lobate grain boundaries) dominate. (e-f) Second-order corridor shear veins: potential early quartz dynamic recrystallisation patterns, expressed by irregular grain boundaries in both extensional and shear veins, are partially overprinted by static recrystallisation referred to as grain boundary area reduction, with typical 120° triple junctions, with smoothly curved grain boundaries and few signs of lattice distortion within the grains.

recrystallised (456 out of 1309 in total; Table 1), though significantly smaller than the relict grains (Figure 8a). Recrystallised grains form a single grain size population (Figure 8a). However, the grain size

distribution is not lognormal as smaller grains are missing, and more than 150 micrometres large, low lattice distortion relict grains are misclassified as recrystallised grains (Figure 8a). We therefore did not

Table 1 – EBSD analysis parameters and post-processing results summarising recrystallised grain characteristics for studied samples. Variables detailed in section 3.2.2.

Structural Control	N-striking, 1 st -order structures		NNE-striking, 2 nd -order structures	
Deposit Name	Antenna	Ancien	Koula	Boulder
Sample	SG41-03	${\bf SG66-05}$	SG72-02	SG437-08
Vein Type	Extensional	Shear-(extensional)	(Shear)-extensional	Shear vein
Step size (µm)	9.8	2.2	3.3	2.2
Map extent (mm^2)	561	20	36	21
Indexing rate $(\%)$	53	83	67	58
Well- vs poorly-constrained grains – cutoff (%) ^a	57	71	15	23
Grains (total count)	1309	6020	2587	6479
Relict grains (count)	456	1235		
Recrystallised grains (count)	853	4785		
Mean grain size diameter (recrystallised grains, μm)	/b	32	63	31
Standard deviation (2σ)	/b	1.9	2.3	4.1

^aPercentage of indexed pixels within a grain to consider it well constrained.

calculate a geometric mean recrystallised grain size for this sample, as it would not be representative of the population (Table 1).

The shear vein sample SG66-05 from drill hole SGDD066 at the Ancien deposit (first-order structure; Figure 1c) shows evidence of subgrain rotation, with elongate subgrains along the S₂ shear fabric, and grain boundary migration, with highly lobate recrystallised grains, as dynamic recrystallisation mechanisms (Figure 7c). Recrystallised grains constitute approximately one-fifth of total grains (1235 out of 6020 in total; Table 1) but occupy a larger volume fraction due to a relatively smaller size difference between relict and recrystallised grains compared to sample SG41-03 (Figure 8b). It should be noted that, although minimal, some artefacts resulting from the stitching of individual EBSD maps prior to post-processing have caused a few grains to be split along map boundaries (Figure 8b). Overall, the recrystallised grain population is unimodal, with a lognormal grain size distribution (geometric mean $=32 \pm 1.9$ micrometres; Table 1).

The extensional vein sample SG72-02 from drill hole SGDD072 at Koula and shear vein sample SG437-08 from drill hole SGRD437 at Boulder (second-order shear corridors; Figure 1c) both display complex, but similar quartz microtextures. Early dynamic recrystallisation, evident from irregular grain boundaries and localised bulge microtextures (Figures 7e, f, 8c) are partially overprinted by 120° triple junctions with smoothly curved grain boundaries and minimal lattice distortion within grains (Figure 7e, f). These features are indicative of grain growth and static recrystallisation processes (Figures 7e, f, 8c, d). Both samples display a lognormal distribution for recrystallised grain size, with geometric means of $64~\pm~2.3$ micrometres for the Koula (shear)-extensional vein (SG72-02) and 31 \pm 2.1 micrometres for the Boulder shear vein (SG437-08; However, lower grain constraint cut-offs of 15% and 23% for these two samples, respectively, somehow reduce reliability of EBSD post-processing data obtained.

Discussion 5

5.1Transpression and strain partitioning at the shear zone scale

This section integrates field and drill core observations the Séguéla gold project to reconstruct the structural evolution of the Séguéla shear zone in the broader tectonic context of the Archean-Paleoproterozoic transition within the sWAC (Figure 1; Eglinger et al., 2017; Chardon et al., 2020; Traoré et al., 2022; Perret et al., 2025). A schematic 3D block diagram (Figure 9) summarises these findings, for deformation postponing the emplacement of the Séguéla bimodal volcanic pile documented by an S_0 pillow bedding (Figure 2a).

5.1.1 D_{1Seg} - D_{2Seg} deformation stages

Relicts of an early, ductile D_{1Seg} deformation stage are preserved as top east-to-the-west thrusts in relatively low-strain rock domains between high-strain shear corridors (Figure 3a). However, identifying structures associated with this early deformation and its kinematics is challenging due to the pervasive overprinting of these features by subsequent deformation. Pre-existing structures are indeed commonly transposed along the high-strain C_2 shear corridors, where newly formed shear band cleavage dominates. Besides, scarcity of oriented drill core data in these lower-strain areas precludes further investigation of D_{1Seg} -related structural features.

The dominant structural framework resulted from a subsequent D_{2Seg} deformation stage. It comprises north-striking, subvertical, high-strain shear corridors, reaching widths of up to a hundred metres. corridors record protracted (brittle)-ductile deformation, marked by coeval development of penetrative S_2 shear band cleavage and associated mineralised quartz veins (Figure 5b, c). The occurrence of deformed shear veins along the S₂ fabric (Figure 5b) and undeformed shear veins developed from crosscutting extensional veins and infilling the S_2 cleavage (Figure 5c) confirms the syn-kinematic nature of vein emplacement during the D_{2Seg} deformation stage. Besides, extensional veins occur predominantly at contacts between lithological

^bNot calculated due to misindexation of some relict grains as recrystallised grains (Figure 8a).

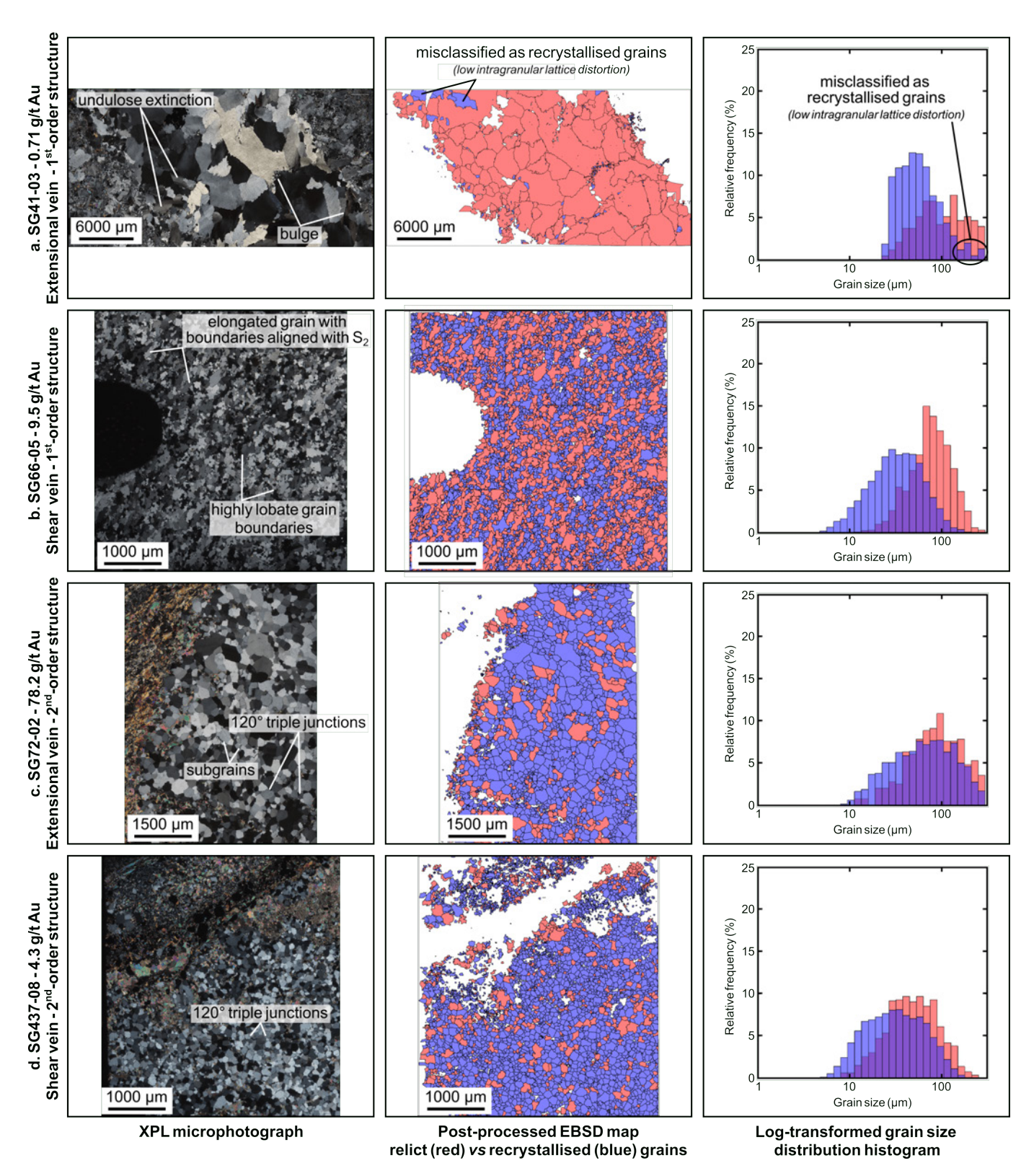


Figure 8 - Comparison of microtextures observed under cross-polarised transmitted light (XPL), the final EBSD map highlighting relict (red) and recrystallised (blue) grains, and the corresponding distribution of recrystallised grain size derived from post-processed EBSD data, following the approach of Cross et al. (2017) as modified by Brochard et al. (2023). White patches on final EBSD maps represent areas of non-indexed pixels corresponding to different mineral phases than quartz. Quartz grain size distribution histograms are based on log-transformed data and illustrate the relative frequencies of relict and recrystallised grains (Cross et al., 2017). (a) Sample SG41-03 - quartz extensional vein along a first-order shear corridor. Some coarse relict grains are misclassified as recrystallised grains due to an intragranular lattice distortion lower than the calculated cut-off for the grain orientation spread (2.5°; Supplementary File 3). (b) Sample SG66-05 - quartz shear vein along a first-order shear corridor. (c) Sample SG72-02 - quartz extensional vein along a second-order shear corridor. (d) Sample SG437-08 quartz shear vein along a second-order shear corridor. Samples SG72-02 and SG437-08 are affected by partial overprinting of quartz microtextures by static recrystallisation.

units, illustrating the critical influence of marked rheological contrasts in facilitating brittle deformation at smaller scales (Figure 5a).

Two geometrically distinct sets of high-strain shear corridors are identified: (i) first-order, north-striking and (ii) second-order, northeast- to north-northeast-striking corridors. The structural relationship between these corridor sets is typified by a jog geometry (Figure 1b, c). Variations in structural elements (e.g., orientation of S₂ cleavage, L₂ stretching lineation, and extensional veins) between first- and second-order corridors highlight strain partitioning during progressive D_{2Seg} deformation, with differing pure and simple shear components:

- (i) Along N000°-N175°-striking first-order shears Sunbird deposit), a subhorizontal L₂ stretching lineation is frequent and indicates block west-to-the-south sinistral-slip shearing. While the presence of subvertical extensional veins is consistent with a strike-slip-dominated regime (Anderson, 1905). their east-northeast-strike deviates the orientation from expected northwest-strike direction. This discrepancy may result from rotation of newly formed extensional veins during prolonged, non-coaxial D_{2Seg} deformation. Alternatively, if these veins have remained unrotated since their formation, their orientation could suggest a local dextral-slip increment within the first-order shear corridor, which is not document by any other kinematic indicators. However, this remains an open question, as assessing vein kinematics is challenging given that observations are limited to drill core data.
- (ii) Along N005°-N010°-striking first-order shears (e.g., Ancien and Antenna deposits), the L_2 stretching lineation is less visible or absent, suggesting a greater pure shear component than at Sunbird. At Antenna, the subhorizontal L₂ lineation also occurs with block west-to-the-south sinistral-slip shearing. Yet, there is also a rare subvertical stretching lineation lying in S_2 shear band cleavage. There is no field evidence supporting that it is relicts of a L_1 stretching lineation in cryptic D_{1Seg} -related thrust planes transposed along the S_2 fabric in high-strain Alternatively, we suggest that shear corridors. the coexistence of subhorizontal to subvertical L₂ stretching lineation and both rare, subvertical and flat extensional veins at Antenna (Figures 3c, 6a) reflect the transition between strike- and dip-slip minor simple shear expressed at local bends along first-order C_2 shear corridors.
- (iii) Along N010°-N045°-striking second-order C₂ shear corridors (e.g., Koula and Boulder deposits), the weakly developed L₂ stretching lineation reflects minor block west-down kinematics. It indicates a dominant flattening strain component with limited simple shear along these second-order shears.

Without definitive markers to quantify displacements or finite strain ellipsoids, the relative contributions of pure and simple shear components to D_{2Seg} deformation remain speculative. However, several lines of evidence suggest the Séguéla shear zone represents a crustal-scale transpressional jog (Figure 9a) resulting from pure shear dominated transpression, such as (i) the presence of S>L tectonites across the shear zone, (ii) vertical S_2 cleavage, oblique to the shear zone and the stretching lineation is vertical along second-order shears, and (iii) flattening as the main finite strain expressed (Sanderson and Marchini, 1984; Fossen et al., 1994; Tikoff and Teyssier, 1994; Dewey et al., 1998). Strain partitioning also occurs along first-order structures, where 5-10° bends in the strike orientation led to transition from sinistral-slip, dip-slip, or no simple shear component of the finite strain expressed. It highlights the crucial angular relationship of structures with convergence angles for predicting strain partitioning in transpressional settings (Leever et al., 2011).

5.1.2Scaling the shear zone structural framework to regional tectonics

Based on the similar strike orientation and apparent kinematics of thrusts observed, the D_{1Seg} deformation stage likely corresponds to northwest-trending oblique convergence during the Eburnean orogeny, that initiated the docking of the Baoulé-Mossi and Kénéma-Man domains from ca. 2135 Ma (Feybesse et al., 1990; Feybesse and Milési, 1994; Masurel et al., 2022; Perret et al., 2025). The D_{2Seg} deformation stage, characterised by block west-to-the-south sinistral-slip kinematics in a transpressional setting, aligns with the 2095-2060 Ma late collisional strike-slip reactivation of major shear zones in the central and western Baoulé-Mossi domain (Caby et al., 2000; Egal et al., 2002; Feybesse et al., 2006; Eglinger et al., 2017; Wane et al., 2018; Perret et al., 2025). Following Fossen et al. (2019), the D_{1Seg} and D_{2Seg} deformation stages may be interpreted as components of a single, progressive deformation phase affecting the central part of the Séguéla greenstone belt (Figure 9b).

This interpretation situates the Séguéla shear zone within the broader framework of the 2135-2120 to 2095 Ma Eburnean Tectonic Event, which culminated in the collision and suturing of the Baoulé-Mossi and Kénéma-Man domains (Perret et al., 2025 and references therein). The overprinting by ca. 2095-2060 Ma late Eburnean transcurrent tectonics, which is the dominant deformation expressed in the studied area, reflects the progressive shift from collisional assembly to late collisional lateral escape, and locally transpression, and crustal reorganisation within the newly formed sWAC (Perret et al., 2025 and references therein). The Séguéla shear zone thus preserves a rare, continuous record of protracted northwest-oriented oblique convergence, capturing both the docking and early cratonisation stages of sWAC evolution. However, the absolute timing of the D_{1Seg} and D_{2Seg} deformation stages cannot be firmly constrained without being speculative, owing to the absence of geochronological data from syn-deformation accessory mineral phases.

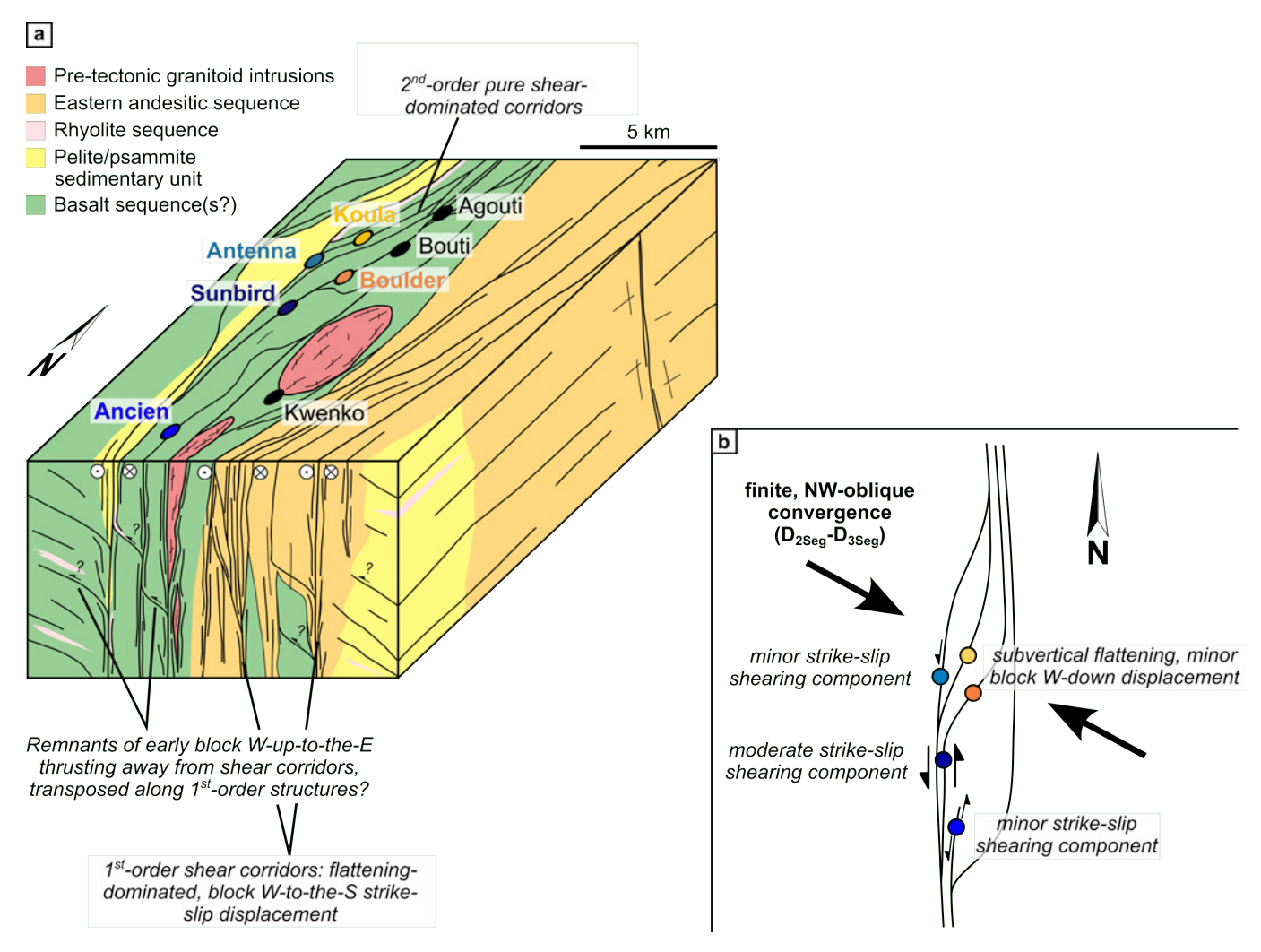


Figure 9 – Crustal-scale transpressional jog in the central Séguéla greenstone belt, centred on the Séguéla gold project (extent in Figure 1b). (a) Schematic 3D block diagram summarising field and core observations, illustrating the distribution of Séguéla gold deposits along both first- and second-order structures. (b) Interpretation of strain partitioning and distribution of flattening vs simple shear strain components between first- and second-order structures across the Séguéla shear zone.

5.1.3 The role of crustal inheritance: insights and research avenues

Strike direction of Séguéla second-order shear corridors matches regional-scale magnetic lineaments to the west (Figure 1b). Although direct field evidence was not observed in this study, the higher density of these northeast-striking structures in the central part of the greenstone belt (Figures 1, 9b) suggests they may have acted as pre-existing zones of weakness favouring the development of the restraining bend. Their oblique alignment with the far-field principal stress direction could have facilitated preferential reactivation, thereby controlling the localisation of the Séguéla transpressional shear zone (e.g., Destro et al., 1994; Worley and Wilson, 1996; Dewey et al., 1998; Cunningham and Mann, 2007). Second, strain is confined to tens of metres to hectometre-scale shear corridors at Séguéla (Figures 1c, 9a), whereas intervening rock volumes exhibit lower strain intensities and preserve primary and early deformation fabrics (Figure 3a). This pattern is consistent with inherited structures acting as strain concentrators, leading to the formation of narrow, localised shear zones while adjacent regions experience

relatively lower strain (e.g., *Holdsworth et al.*, 1997; *Rutter et al.*, 2001; *Torgersen and Viola*, 2014).

However, questions remain about the origin and timing of these likely inherited, northeast-striking structures, i.e., whether they formed as neo-tectonic features during the early Eburnean orogeny or were reactivated remnants of Archean lithospheric architecture. An integrated multimethod approach combining fieldwork to deep-penetrating geophysics and U-Pb-Hf-O isotopic analyses is necessary to resolve these uncertainties regarding crustal inheritance's role in strain localisation and structural evolution across the Archean-Paleoproterozoic transition zone of the sWAC.

5.2 Strain partitioning at the microscopic scale

5.2.1 Dynamic vs static recrystallisation mechanisms along first- and second-order structures

Quartz undergoes dynamic recrystallisation primarily by three temperature- and strain rate-dependent mechanisms, i.e., bulge recrystallisation (relatively

high strain rate), temperature, subgrain rotation recrystallisation (intermediate temperature, intermediate strain rate) and grain boundary migration recrystallisation (high temperature, lower strain rate; Passchier and Trouw, 2005 and references therein). These mechanisms form a continuum and can occur simultaneously during deformation (*Lloyd and Freeman*, 1994). Classification of the observed microtextures into these recrystallisation mechanisms was informed by numerous studies (White, 1977; Drury and Urai, 1990; Gifkins, 1994; Trimby et al., 1998; Stipp et al., 2002a,b; Stipp and Kunze, 2008; Platt and Behr, 2011; Xia and Platt, 2018). When deformation stops at relatively high temperature or in the presence of enough water along grain boundaries, static recrystallisation may occur to reach a lower internal energy configuration (Evans et al., 2001; Passchier and Trouw, 2005). The main mechanism responsible for such a grain recovery is grain boundary area reduction, characterised by coarser, strain-free quartz grains (i.e., without undulose extinction or subgrains) with straight or smoothly curved grain boundaries forming 120° triple junctions (Passchier and Trouw, 2005 and references therein).

Microscopic and EBSD analyses of quartz-dominated mineralised veins from deposits along the first- and second-order structures of the Séguéla shear zone revealed contrasting recrystallisation styles. Quartz veins associated with first-order shear corridors preserve predominantly dynamic recrystallisation textures (i.e., bulge recrystallisation, elongate subgrains or highly lobate grain boundaries), while static recrystallisation textures (i.e., 120° triple junctions between smoothly curved grain boundaries) overprint earlier dynamic recrystallisation expression in veins along second-order shear corridors (Figures 7, 8). Several observations support contemporaneous quartz recrystallisation and veining during protracted D_{2Seg} deformation: (i) quartz recrystallisation affects all studied veins, (ii) dynamically recrystallised grains via subgrain rotation in shear veins are preferentially elongated along the S₂ shear cleavage trace in sections (Figure 7c, d), (iii) no significant post-veining deformation overprints veins or adjacent host rocks, and (iv) static recrystallisation is not widespread across all quartz veins along first- and second-order structures, precluding post-deformation recovery as a plausible explanation. Therefore, the differential quartz recrystallisation patterns recorded in quartz veins in first- and second-order structures reflect deformation conditions during the development of the Séguéla transpressional shear zone.

5.2.2Insights into strain intensity partitioning and long- vs short-lived deformation

interplay between dynamic and static recrystallisation of quartz is influenced by factors such as temperature, strain rate and intensity, alternance between active deformation and relaxation (Hirth and Tullis, 1992; Passchier and Trouw, 2005), and also rock matrix properties (e.g., Papa et al., 2020). In the present study, the matrix composition remains constant across all vein types and structural contexts, with veins composed of similar mineral assemblages. Although mineralised vein arrays may develop within or at contacts between different units (see section 2.3.2), all studied samples are hosted by the same basaltic unit. This suggests that rheological contrasts between host units do not play a significant role in the local-scale veining dynamics here. Furthermore, there is no evidence for significant temperature variations between first- and second-order structures, as indicated by the absence of changes in host rock mineral assemblages that would reflect differing metamorphic grades. Nonetheless, temperature conditions along the various structures of the Séguéla shear zone remain poorly constrained.

thus infer that the differential quartz recrystallisation patterns recorded in quartz veins in first- and second-order structures is driven by variations in strain intensity, strain rate and/or duration of deformation within the Séguéla transpressional shear zone. First-order structures likely experienced sustained high strain intensity and strain rates under relatively stable deformation conditions through time, promoting continuous dynamic recrystallisation and inhibiting static processes (e.g., Wheeler et al., 2004; Papa et al., 2020). The smaller recrystallised grain sizes observed in shear veins compared to extensional veins suggest that higher local flow stresses were involved in their formation (Table 1). These differences likely reflect local variations in stress, strain rate, and/or temperature distribution during the prolonged D_{2Seg} deformation (*Twiss*, 1977; Stipp et al., 2002b; Stipp and Kunze, 2008). Conversely, in mineralised veins along second-order structures, early dynamic recrystallisation microtextures are overprinted by grain growth recovery processes, as characterised by a lognormal grain size distribution (Figure 8c and d; Okazaki and Conrad, 1972). Transient D_{2Seg} deformation with intervening periods of thermal or strain relaxation may have facilitated the overprint of static recrystallisation textures in quartz (e.g., Chamlagain and Hayashi, 2007).

The static recrystallisation features observed in second-order structures are therefore interpreted as meta-dynamic, i.e., quartz grain recovery processes immediately postdated dynamic recrystallisation affecting the veins along second-order structures during D_{2Seg} deformation. This overprint may reflect either limited deformation recorded by mineralised veins in second-order shear zones relative to first-order structures, or more transient deformation conditions affecting second-order structures compared to the more sustained deformation within first-order ones. The latter hypothesis is supported by the lack of primary vein microstructures (e.g., fibrous, blocky-elongate quartz) preserved in quartz veins from second-order shear zones, and by the absence of clear evidence for lower strain in the host rock, except for a narrower damage zone and reduced volume of affected rock (Figure 9a). In any case, whether the observed transition in recrystallisation mechanisms reflects a shift from long- to short-lived deformation, or a change in strain intensity, the two interpretations are not mutually exclusive. Together,

they offer valuable insights into the partitioning of the D_{2Seg} deformation across the Séguéla transpressional jog.

5.3 Influence of strain partitioning on ore formation

Deciphering structurally controlled hydrothermal gold mineralisation remains challenging due to complex interactions among deformation processes, host-rock rheology, and fluid dynamics over potentially protracted and/or polyphased mineralisation histories (e.g., Blenkinsop et al., 2020). Here, we highlight how understanding strain partitioning within the Séguéla shear zone allows for predicting the distribution, grade and tonnage of deposits in the Séguéla gold project, and orientation of ore shoots at the deposit scale.

Influence on deposit distribution 5.3.1

Gold deposits within the Séguéla shear zone primarily occur around a restraining bend, consistent with the global observation that mineralisation typically localises within jogs or bends, while straight shear segments tend to remain barren (e.g., Groves et al., 2018). However, Séguéla mineralisation also extends along the bounding first-order shear zones, beyond the bend itself (Figures 1c, 9a).

distribution partially contrasts with the conventional model, in which first-order faults predominantly act as major fluid conduits, controlling deposit size, whereas smaller-scale, second- and third-order structures such as bends, stepovers, and splays, serve as preferred sites for ore deposition within an overall compressive regime, controlling orebody geometry and grade (e.g., Groves et al., 2018). Nevertheless, Séguéla gold deposit distribution aligns well with numerical models indicating that permeability enhancement through coseismic damage is not confined to the stepover region but can propagate into the adjacent wall rocks (Micklethwaite et al., 2015). Specifically, areas of greatest Coulomb stress reduction predicted for a restraining, overlapping stepover geometry, with first-order shear zones oriented around 60° to the far-field shortening direction (see Figures 6 and 7 in Micklethwaite et al., 2015), coincide precisely with the Séguéla shear zone configuration and deposit distribution (Figure 9b). In these areas, repeated transient fault reactivation driven by fluid overpressure likely promoted fault-valve behaviour and associated gold deposition (Sibson, 1990, 1992; Micklethwaite et al., 2015; Sibson, 2020). The findings of this study thus underscore the critical importance of detailed investigations of strain partitioning across transpressional shear zones for district-scale exploration targeting of orogenic gold from the Archean to the Phanerozoic (Sibson and Scott, 1998; Miller et al., 2000; Chen, 2001; Bateman and Bierlein, 2007; Zoheir, 2011; Lawley et al., 2013; El-Wahed et al., 2016; Lacroix et al., 2020; Perret et al., 2021; Hauteville et al., 2025), as well as other types of deposits (Martín-Izard et al., 2002; Seymour et al., 2024; Yan et al., 2024).

5.3.2 Influence on deposit grade and tonnage

The Séguéla first-order shear zones host more numerous and richer gold deposits (higher cumulative tonnage and average gold grade) compared to second-order structures (Table 2). The higher gold endowment along first-order structures likely reflects increased deformation intensity, as evidenced by quartz vein microtextures indicating sustained dynamic recrystallisation in mineralised veins compared to second-order structures. strain along first-order structures presumably facilitated repeated seismic cycles, promoting episodic permeability enhancement and fault-valve fluid conducive to efficient gold deposition (Sibson, 1990, 1992, 2004, 2020). Again, this deviates somewhat from the classical model of deposit size, geometry and grade distribution across firstand second-order structures.

The Koula deposit constitutes a notable exception with respect to grade, owing to its unique geological context within a second-order shear corridor limited to 15 metres in width, featuring stacked quartz veins on intervals up to 10 metres in thickness (Weedon et al., 2023). The combined evidence for enhanced mineralising fluid flow along the Koula shear zone, together with its relatively narrow width, supports a model of pronounced strain localisation within a mechanically weakened shear zone (e.g., Cawood and Platt, 2021), potentially resulting from the reactivation of a pre-existing crustal structure (see subsection 5.1.3). Overall, the Séguéla case still demonstrates the significance of deformation intensity in both first- and second-order shear zones for predicting gold deposit grade and tonnage depending on their distribution in transpressional settings.

5.3.3 Additional, deposit-scale controls on ore distribution

The strike orientation of first-order shear zones bounding the western side of the Séguéla shear zone progressively rotates by approximately 10-15°, from N005°-N010° at Antenna and Ancien to N000°-N175° at Sunbird (Figures 4, 9). This curvature and its relationship with the far-field shortening direction enhance the strike-slip component of D_{2Seg} deformation at Sunbird compared to Antenna and Ancien (Figure 9). At Sunbird, subvertical intersections between extensional and shear veins likely control the ore shoot geometry (Figure 6), correlating well with its substantial underground resource potential, unequalled in the Séguéla gold project (Table 2). Such an orientation reflects local dilational zones preferentially developed at Sunbird, favoured by the intermediate principal stress (σ_2) in an Andersonian strike-slip regime (Figure 9). σ_2 is indeed known to favour dilation zones acting as long-lived conduits for auriferous fluids in different tectonic regimes, consistent with fault-valve fluid-flow model (Anderson, 1905; Peters, 1993; Sibson and Scott, 1998; Sibson, 2004; Cox, 2005, 2020).

Additionally, the Antenna deposit uniquely occurs at a major, sheared lithological contact between a competent rhyolite unit to the west and a softer basaltic sequence to the east (Figure 1b, c; section

Table 2 – Mineral reserves and resources of the Séguéla gold project, modified from Weedon et al. (2023). Deposits are categorised by their location along north-striking first-order and northeast-striking second-order shear zones.

Structural Control	N-striking, 1 st -order structures			NNE-striking, 2 nd -order structures				
Deposit Name	Antenna	Ancien	Sunbird	Agoutia	Koula	Boulder		
Probable Reserves								
Cut-off grade (g/t Au)	0.65	0.73	0.66	0.72	0.66	0.69		
Tonnage (Mt)	4.4	1.8	2.1	0.90	1.5	0.71		
Grade (g/t Au)	2.3	3.8	3.0	2.4	5.8	1.7		
Metal (koz t Au)	$321 \mid 10.0$	$221 \mid 6.9$	$206 \mid 6.4$	$70 \mid 2.2$	$268 \mid 8.3$	$206 \mid 6.4$		
Indicated Resources - Open Pit (Exclusive of Mineral Reserve Estimate)								
Cut-off grade (g/t Au)	0.55	0.65	0.55	0.65	0.60	0.60		
Tonnage (Mt)	1.3	0.19	0.55	0.30	0.05	0.43		
Grade (g/t Au)	1.3	2.8	1.8	1.7	5.8	1.1		
Metal (koz t Au)	$57 \mid 1.8$	$17 \mid 0.53$	$31 \mid 0.96$	$16 \mid 0.50$	$10 \mid 0.31$	$16 \mid 0.50$		
Indicated Resources - Underground (Exclusive of Mineral Reserve Estimate)								
Cut-off grade (g/t Au)		2.4	2.4		2.4			
Tonnage (Mt)		0.19	1.6		0.04			
Grade (g/t Au)		3.8	4.1		4.5			
Metal (koz t Au)		$23 \mid 0.72$	203 6.3		$7 \mid 0.22$			
Total - Probable Reserves + Indicated Resources								
Tonnage (Mt)	5.7	2.2	4.3	1.2	1.6	1.1		
Grade (g/t Au)	2.1	3.7	3.3	2.2	5.8	1.5		
Metal (koz t Au)	$378 \mid 11.8$	$261 \mid 8.1$	$440 \mid 13.7$	$86 \mid 2.7$	$285 \mid 8.9$	222 6.9		

^aNot studied, located in Figure 1b.

2.3.2). This significant rheological contrast influences strain localisation, deformation intensity, and fluid flow pathways, focusing deformation and promoting favourable sites for mineralisation (Blenkinsop et al., 2020 and references therein). Such rheological differences likely underpin Antenna's substantial gold endowment, representing the largest deposit at Séguéla (Table 2). Thus, besides strain partitioning at the crustal scale, local controls such as subtle structural curvature and host rock rheology significantly affect gold mineralisation distribution within complex, crustal-scale shear systems.

Conclusion

This study investigates the interplay between transpressional deformation, strain partitioning, and structural inheritance within the gold-endowed, crustal-scale Séguéla shear zone, using an integrated approach combining field, drill core, microscopic observations, and EBSD analysis of mineralised quartz veins. An early D_{1Seg} deformation stage, characterised by ductile thrusting, is preserved only within isolated, low-strain domains, having been largely overprinted by the subsequent D_{2Seg} stage. This protracted ductile-(brittle) D_{2Seg} stage established the structural framework of the shear zone, primarily through north-striking, subvertical first-order shear corridors dominated by pure shear transpression with variable sinistral strike-slip or dip-slip components. partitioning along subtle 5-10° bends within these corridors is evidenced by changes in stretching lineation orientations and coeval extensional vein orientations. Conversely, second-order northeast-striking corridors accommodated mostly flattening with limited simple shear components, resulting in

pronounced S>L tectonites. Mineralised extensional, shear-extensional, and shear veins formed concurrently along these first- and second-order structures during the D_{2Seg} deformation stage, hosting significant gold deposits at Séguéla. Regionally, the D_{1Seg} and D_{2Seg} stages represent progressive deformation reflecting northwest-directed oblique convergence and strike-slip reactivation during the Paleoproterozoic Eburnean orogeny in the sWAC. Nevertheless, the timing and exact influence of potentially inherited, northeast-striking structures in localising the Séguéla shear zone remain uncertain.

Quartz recrystallisation patterns differ notably between veins hosted by first- and second-order shear corridors due to variations in strain intensity and/or deformation duration. Veins along first-order structures predominantly record dynamic recrystallisation, indicative of sustained high-strain deformation. In contrast, veins within second-order structures exhibit partial static recrystallisation, reflecting strain relaxation dominating over transient deformation.

Strain partitioning within the Séguéla transpressional shear zone significantly influenced the spatial distribution, grade, and tonnage of gold deposits along first- and second-order structures. Deposits are preferentially localised within low Coulomb-failure stress regions, particularly in and adjacent to the restraining bend region, aligning closely with predictions from numerical modelling. Variations in gold endowment correlate directly with deformation intensity and/or duration of activity, with first-order shear corridors generally hosting richer and larger deposits. elevated underground resource potential at Sunbird reflects increased local strike-slip deformation, while

Antenna, the district's largest deposit, exemplifies preferential strain localisation facilitated by the strong rheological contrast between competent rhyolite and softer basalt units.

Overall, the Séguéla shear zone provides a compelling example illustrating the critical importance of detailed, multiscale strain partitioning analysis within transpressional shear systems, contributing significantly to tectonic reconstruction and informing district-scale mineral exploration strategies.

Acknowledgements

This study has been conducted as part of the stage 4 of the West African exploration Initiative project (WAXI4, P934C), supported by AMIRA International, industry sponsors, and in kind-sponsors. DF acknowledges financial support from the Australian Research Council (FT240100041). JP is grateful to the staff of Fortuna Silver and Roxgold SANGO on and off site for providing any human, logistic and scientific support needed during fieldwork at Séguéla. Special thanks go to M.B. Dia, M. Bossé, R. Aké, I. Sidibé, B. Podet, P. Weedon, A. Nouhoum, H. Parry, P. McLean, and the exploration tech crew for daily help at the core shack. S. Zapata and G. Zeilinger are warmly thanked for their comments that helped to improve the manuscript. We also thank C. Magee and M. Gouiza for editorial handling, and R. Stanca for article copyediting and production.

Author contributions

Fieldwork, conceptualisation, data analysis, figure creation, and manuscript writing were conducted by JP. Additional fieldwork was conducted by PCH. EBSD analyses were performed by DF, while EBSD post-processing was carried out by JP and CB. Project funding was secured by MWJ and NT. NT, DF, CB, PCH and MWJ contributed to the editing and review of the manuscript.

Data availability

Supplementary files are available on a Zenodo repository: https://zenodo.org/records/15036789

Competing interests

The authors declare no competing interests.

Peer review

This publication was peer-reviewed by Gerold Zeilinger and Sebastian Zapata. The full peer-review report can be found here: Review Report.

Copyright notice

© Author(s) 2025. This article is distributed under the Creative Commons Attribution 4.0 International License, which permits unrestricted use, distribution, and reproduction in any medium, provided the original author(s) and source are credited, and any changes made are indicated.

References

- Allialy, M. E., B. R. Kouassi, N. N. Houssou, F. J. L. Kouadio, D. B. Siogbo, and F. O. Konan (2023), Fouimba and Goma mounts Greenstone belts litho-structural analysis related to Côte D'Ivoire birimian geodynamic setting and implying in west-Africa craton gold deposits, Journal of Geoscience and Environment Protection, 11(01), 150–168, https://doi.org/10.4236/gep.2023.111010.
- Amoih, L. Y. K. (2022), Etude lithostratigraphique et géochimique du projet aurifère de Séguéla, Master's thesis, Université Félix Houphouet-Boigny, Abidjan, Côte d'Ivoire.
- Anderson, E. M. (1905), The dynamics of faulting, Transactions of the Edinburgh Geological Society, 8(3), 387–402, https://doi.org/10.1144/transed.8.3.387.
- Bachmann, F., R. Hielscher, and H. Schaeben (2010), Texture analysis with MTEX free and open source software toolbox, *Solid State Phenomena*, 160, 63–68, https://doi.org/10.4028/www.scientific.net/ssp.160.63.
- Bachmann, F., R. Hielscher, and H. Schaeben (2011), Grain detection from 2d and 3d EBSD data–specification of the MTEX algorithm, *Ultramicroscopy*, 111(12), 1720–1733, ht tps://doi.org/10.1016/j.ultramic.2011.08.002.
- Baratoux, L., V. Metelka, S. Naba, M. W. Jessell, M. Grégoire, and J. Ganne (2011), Juvenile Paleoproterozoic crust evolution during the Eburnean orogeny (~2.2–2.0 Ga), western Burkina Faso, Precambrian Research, 191(1-2), 18–45, https://doi.org/10.1016/j.precamres.2011.08.010.
- Baratoux, L., M. W. Jessell, and A. N. Kouamelan (2024), The west African craton, in *Regional Geology Reviews*, edited by Z. Hamimi, M. C. Chabou, E. Errami, A.-R. Fowler, N. Fello, A. Masrouhi, and R. Leprêtre, pp. 47–68, Springer International Publishing, Cham, https://doi.org/10.1007/978-3-031-48299-1_3.
- Bateman, R., and F. P. Bierlein (2007), On Kalgoorlie (Australia), Timmins–Porcupine (Canada), and factors in intense gold mineralisation, *Ore Geology Reviews*, 32(1-2), 187–206, https://doi.org/10.1016/j.oregeorev.2006.08.001.
- Beach, A. (1977), Vein arrays, hydraulic fractures and pressure-solution structures in a deformed flysch sequence S.W. England, *Tectonophysics*, 40(3-4), 201–225, https://doi.org/10.1016/0040-1951(77)90066-x.
- Bessoles, B. (1977), Géologie de l'Afrique: le craton ouest africain, Mémoires du Bureau de Recherches Geologiques et Minières, vol. 88, BRGM.
- Blenkinsop, T. G., N. H. S. Oliver, P. G. H. M. Dirks, M. Nugus, G. Tripp, and I. Sanislav (2020), Chapter 1: Structural geology applied to the evaluation of hydrothermal gold deposits, in *APPLIED STRUCTURAL GEOLOGY OF ORE-FORMING HYDROTHERMAL SYSTEMS*, edited by J. V. Rowland and D. A. Rhys, pp. 1–23, Society of Economic Geologists, https://doi.org/10.5382/rev.21.01.

- Boher, M., W. Abouchami, A. Michard, F. Albarède, and N. Arndt (1992), Crustal growth in west Africa at 2.1 Ga, *Journal of Geophysical Research, Solid Earth*, 97(B1), 345–369, https://doi.org/10.1029/91JB01640.
- Bonhomme, M. (1962), Contribution à l'étude géochronologique de la plate-forme de l'Ouest Africain, Imprimerie Louis-Jean.
- Bons, P. (2000), The formation of veins and their microstructures, *Journal of the Virtual Explorer*, 02, 12, https://doi.org/10.3809/JVIRTEX.2000.00007.
- Bons, P. D., and M. W. Jessell (1997), Experimental simulation of the formation of fibrous veins by localised dissolution-precipitation creep, *Mineralogical Magazine*, 61(404), 53–63, https://doi.org/10.1180/minmag.1997.061.404.06.
- Bons, P. D., M. A. Elburg, and E. Gomez-Rivas (2012), A review of the formation of tectonic veins and their microstructures, *Journal of Structural Geology*, 43, 33–62, https://doi.org/10.1016/j.jsg.2012.07.005.
- Bons, P. D., D. Cao, T. de Riese, E. González-Esvertit, D. Koehn, I. Naaman, T. Sachau, H. Tian, and E. Gomez-Rivas (2022), A review of natural hydrofractures in rocks, *Geological Magazine*, pp. 1–26, https://doi.org/ 10.1017/s0016756822001042.
- Brochard, C. (2022), Paléo-contraintes et origine des fluides des veines orogéniques de la ceinture de roches vertes de l'Abitibi, Master's thesis, Université du Québec à Montréal, Montreal, Canada.
- Brochard, C., M. Jébrak, and S. De Souza (2023), Deformation and paleopiezometry of auriferous quartz veins in Archean orogenic gold deposits of the Abitibi greenstone belt, *Journal of Structural Geology*, 177(104986), 104,986, https://doi.org/10.1016/j.jsg.2023.104986.
- Bürgmann, R., and D. D. Pollard (1992), Influence of the state of stress on the brittle-ductile transition in granitic rock: Evidence from fault steps in the Sierra Nevada, California, *Geology*, 20(7), 645, https://doi.org/10.113 0/0091-7613(1992)020<0645:IOTSOS>2.3.CO;2.
- Bürgmann, R., and D. D. Pollard (1994), Strain accommodation about strike-slip fault discontinuities in granitic rock under brittle-to-ductile conditions, *Journal of Structural Geology*, 16(12), 1655–1674, https://doi.org/10.1016/0191-8141(94)90133-3.
- Caby, R., C. Delor, and O. Agoh (2000), Lithologie, structure et métamorphisme des formations birimiennes dans la région d'Odienné(Co^te d'Ivoire): ro^le majeur du diapirisme des plutons et des décrochements en bordure du craton de Man, Journal of African Earth Sciences, 30(2), 351–374, https://doi.org/10.1016/S0899-5362(00)00024-5.
- Cawood, T. K., and J. P. Platt (2021), What controls the width of ductile shear zones?, *Tectonophysics*, 816(229033), 229,033, https://doi.org/10.1016/j.tecto. 2021.229033.
- Cerchiari, A., F. Remitti, S. Mittempergher, A. Festa, F. Lugli, and A. Cipriani (2020), Cyclical variations of fluid sources and stress state in a shallow megathrust-zone mélange, *Journal of the Geological Society*, 177(3),

- 647-659, https://doi.org/10.1144/jgs2019-072.
- Chamlagain, D., and D. Hayashi (2007), Finite strain variation across the Mahabharat Thrust in central Nepal Himalaya, *Journal of Nepal Geological Society*, 35, 11–20, https://doi.org/10.3126/jngs.v35i0.23630.
- Chardon, D., O. Bamba, and K. Traoré (2020), Eburnean deformation pattern of Burkina Faso and the tectonic significance of shear zones in the West African craton, Bulletin de la Societe Geologique de France, 191(1), 2, https://doi.org/10.1051/bsgf/2020001.
- Chen, S. (2001), Transpression and restraining jogs in the northeastern Yilgarn craton, Western Australia, *Precambrian Research*, 106(3-4), 309–328, https://doi.org/10.1016/s0301-9268(00)00138-8.
- Choulet, F., M. Faure, D. Cluzel, Y. Chen, W. Lin, and B. Wang (2012), From oblique accretion to transpression in the evolution of the Altaid collage: New insights from West Junggar, northwestern China, *Gondwana Research*, 21(2-3), 530–547, https://doi.org/10.1016/j.gr.2011.07.0 15.
- Cox, S. (2005), Coupling between Deformation, Fluid Pressures, and Fluid Flow in Ore-Producing Hydrothermal Systems at Depth in the Crust, Economic Geology; Bulletin of the Society of Economic Geologists, 100, 39–75.
- Cox, S., V. Wall, M. Etheridge, and T. F. Potter (1991), Deformational and metamorphic processes in the formation of mesothermal vein-hosted gold deposits examples from the Lachlan Fold Belt in central Victoria, Australia, *Ore Geology Reviews*, 6(5), 391–423, https://doi.org/10.1016/0169-1368(91)90038-9.
- Cox, S., M. Knackstedt, and J. Braun (2001), Principles of structural control on permeability and fluid flow in hydrothermal systems, in *Structural Controls on Ore Genesis*, *Reviews in Economic Geology*, vol. 14, edited by J. P. Richards and R. M. Tosdal, pp. 1–22, Society of Economic Geologists, https://doi.org/10.5382/rev.14.01.
- Cox, S. F. (2010), The application of failure mode diagrams for exploring the roles of fluid pressure and stress states in controlling styles of fracture-controlled permeability enhancement in faults and shear zones, *Geofluids*, 10(1-2), 217–233, https://doi.org/10.1111/j.1468-8123.2010.00281.x.
- Cox, S. F. (2020), Chapter 2: The Dynamics of Permeability Enhancement and Fluid Flow in Overpressured, Fracture-Controlled Hydrothermal Systems, in *APPLIED STRUCTURAL GEOLOGY OF ORE-FORMING HYDROTHERMAL SYSTEMS*, Society of Economic Geologists, https://doi.org/10.5382/rev.21.02.
- Cox, S. F., and K. Ruming (2004), The St Ives mesothermal gold system, Western Australia—a case of golden aftershocks?, *Journal of Structural Geology*, 26(6-7), 1109–1125, https://doi.org/10.1016/j.jsg.2003.11.025.
- Criddle, P., H. Andersen, P. Weedon, D. Morgan, G. Bailey, S. McLeay, and N. Morrison (2021), Séguéla Project, Feasibility Study, Worodougou Region, Côte d'Ivoire, *Tech. rep.*, RoxGold.
- Cross, A., S. Kidder, and D. Prior (2015), Using microstructures and TitaniQ thermobarometry of quartz

- sheared around garnet porphyroclasts to evaluate microstructural evolution and constrain an Alpine Fault Zone geotherm, Journal of Structural Geology, 75, 17–31, https://doi.org/10.1016/J.JSG.2015.02.012.
- Cross, A. J., D. J. Prior, M. Stipp, and S. Kidder (2017), The recrystallized grain size piezometer for quartz: An EBSD-based calibration, Geophysical Research Letters, 44(13), 6667-6674, https://doi.org/10.1002/2017gl073836.
- Cunningham, W. D., and P. Mann (2007), Tectonics of strike-slip restraining and releasing bends, Geological Society Special Publication, 290(1), 1-12, https://doi.or g/10.1144/SP290.1.
- del Real, I., R. W. Allmendinger, J. F. H. Thompson, and C. Creixell (2023), Evidence for transpression during formation of the Candelaria Punta del Cobre IOCG -district and regional implications, Journal of South American Earth Sciences, 126(104289), 104,289, https: //doi.org/10.1016/j.jsames.2023.104289.
- Destro, N., P. Szatmari, and E. A. Ladeira (1994), Post-Devonian transpressional reactivation Proterozoic ductile shear zone in Ceará, NEBrazil, Journal of Structural Geology, 16(1), 35-45, https://doi.org/10.1016/0191-8141(94)90016-7.
- Dewey, J. F., R. E. Holdsworth, and R. A. Strachan (1998), Transpression and transtension zones, Geological Society Special Publication, 135(1), 1–14, https://doi.org/10.114 4/GSL.SP.1998.135.01.01.
- Diraison, M., P. R. Cobbold, E. A. Rossello, and A. J. Amos (1998), Neogene dextral transpression due to oblique convergence across the Andes of northwestern Patagonia, Argentina, Journal of South American Earth Sciences, 11(6), 519-532, https://doi.org/10.1016/s0895-9811(98)00032-7.
- Drury, M., and J. Urai (1990), Deformation-related recrystallization processes, *Tectonophysics*, 172(3-4), 235-253, https://doi.org/10.1016/0040-1951(90)90033-5.
- Dubé, B., and P. Gosselin (2007), Greenstone-hosted quartz-carbonate vein deposits, in Geological Association of Canada, Mineral Deposits Division, Special Publication, Special Publication, geological association of canada, mineral deposits division ed., pp. 49-73, Goodfellow W.D.
- Egal, E., D. Thiéblemont, D. Lahondère, C. Guerrot, C. A. Costea, D. Iliescu, C. Delor, J.-C. Goujou, J. Lafon, M. Tegyey, S. Diaby, and P. Kolié (2002), Late Eburnean granitization and tectonics along the western and northwestern margin of the Archean Kenema-Man domain (Guinea, West African Craton), Precambrian Research, 117(1-2), 57-84, https://doi.org/10.1016/S0301-9268(02)00060-8.
- Eglinger, A., N. Thébaud, A. Zeh, J. Davis, J. Miller, L. A. Parra-Avila, R. Loucks, C. McCuaig, and E. Belousova (2017), New insights into the crustal growth of the Paleoproterozoic margin of the Archean Kéména-Man domain, West African craton (Guinea): Implications for gold mineral system, Precambrian Research, 292, 258–289, https://doi.org/10.1016/j.precamres.2016.11.012.
- El-Wahed, M., H. Harraz, and M. El-Behairy (2016), Transpressional imbricate thrust zones controlling gold

- mineralization in the Central Eastern Desert of Egypt, Ore Geology Reviews, 78, 424–446, https://doi.org/10.1016/J. OREGEOREV.2016.03.022.
- Ephrem, A. M., H. N. Nestor, K. F. J. Luc, D. B. Siogbo, K. B. Roland, and K. H. Felix (2023), Litho-structural and geochemistry analysis of granitoids from mount fouimba and Goma in seguela area (central-western Côte d'Ivoire), Open Journal of Geology, 13(01), 72-89, https://doi.org/ 10.4236/ojg.2023.131004.
- Etheridge, M. (1983), Differential stress magnitudes during regional deformation and metamorphism: Upper bound imposed by tensile fracturing, Geology, 11(4), 231-234, https://doi.org/10.1130/0091-7613(1983)11<231: DSMDRD>2.0.CO;2.
- Evans, B., J. Renner, and G. Hirth (2001), A few remarks on the kinetics of static grain growth in rocks, International Journal of Earth Sciences, 90, 88–103, https://doi.org/10 .1007/S005310000150.
- Feybesse, J., and J. Milési (1994), The Archaean/Proterozoic contact zone in West Africa: a mountain belt of décollement thrusting and folding on a continental margin related to 2.1 Ga convergence of Archaean cratons?, Precambrian Research, 69(1-4), 199-227, https://doi.or g/10.1016/0301-9268(94)90087-6.
- Feybesse, J., J. Milési, V. Johan, A. Dommanget, J.-Y. Calvez, M. Boher, and W. Abauchami (1989), La limite Archéen/Protérozoïque inférieur d'Afrique de l'Ouest: une zone de chevauchement majeure antérieure à l'accident de Sassandra; l'exemple des régions d'Odiénné et de Touba (Côte-d'Ivoire), Comptes Rendus de l'Académie des Sciences. Série 2, Mécanique, Physique, Chimie, Sciences de l'univers, Sciences de la Terre, 309(18), 1847-1853.
- Feybesse, J., J. Milési, P. Verhaeghe, and V. Johan (1990), Le domaine de Toulepleu-Ity (Côte-d'Ivoire); une unité «birrimienne» charriée sur les gneiss archéens du domaine de Kénéma-Man lors des premiers stades de l'orogène éburnéen, Comptes Rendus de l'Académie des Sciences. Série 2, Mécanique, Physique, Chimie, Sciences de l'univers, Sciences de la Terre, 310(3), 285-291.
- Feybesse, J., M. Billa, C. Guerrot, E. Duguey, J. Lescuyer, J. Milési, and V. Bouchot (2006), The paleoproterozoic Ghanaian province: Geodynamic model and ore controls, including regional stress modeling, Precambrian Research, 149(3-4), 149–196, https://doi.org/10.1016/J.PRECAM RES.2006.06.003.
- Fossen, H., and B. Tikoff (1998), Extended models of transpression and transtension, and application to tectonic settings, Geological Society Special Publication, 135(1), 15-33, https://doi.org/10.1144/gsl.sp.1998.135.01.02.
- Fossen, H., B. Tikoff, C. Teyssier, and H. Fossen (1994), Strain modeling of transpressional and transtensional deformation, Norsk Geologisk Tidsskrift, 74, 134–145.
- Fossen, H., G. C. G. Cavalcante, R. V. L. Pinheiro, and C. J. Archanjo (2019), Deformation – progressive or multiphase?, Journal of Structural Geology, 125, 82–99, https://doi.org/10.1016/j.jsg.2018.05.006.
- Gifkins, R. C. (1994), Grain-boundary participation in high-temperature deformation: An historical review,

- Materials Characterization, 32(2), 59-77, https://doi.org/10.1016/1044-5803(94)90093-0.
- Gremmel, J., G. Duclaux, M. Corsini, and J. Bascou (2024), Constrictional flow and strain partitioning during oblique deformation: Insights from the Variscan Tanneron Massif, SE France, *Tektonika*, 2(2), 112–140, https://doi.org/10.5 5575/tektonika2024.2.2.69.
- Grenholm, M. (2019), The global tectonic context of the ca. 2.27-1.96 Ga Birimian Orogen Insights from comparative studies, with implications for supercontinent cycles, *Earth-Science Reviews*, 193, 260–298, https://doi.org/10.1016/j.earscirev.2019.04.017.
- Grenholm, M., M. Jessell, and N. Thébaud (2019a), Paleoproterozoic volcano-sedimentary series in the ca. 2.27–1.96 Ga Birimian Orogen of the southeastern West African Craton, *Precambrian Research*, 328, 161–192, https://doi.org/10.1016/j.precamres.2019.04.005.
- Grenholm, M., M. Jessell, and N. Thébaud (2019b), A geodynamic model for the Paleoproterozoic (ca. 2.27–1.96 Ga) Birimian Orogen of the southern West African Craton Insights into an evolving accretionary-collisional orogenic system, *Earth-Science Reviews*, 192, 138–193, https://doi.org/10.1016/j.earscirev.2019.02.006.
- Groves, D. I., M. Santosh, R. J. Goldfarb, and L. Zhang (2018), Structural geometry of orogenic gold deposits: Implications for exploration of world-class and giant deposits, *Geoscience Frontiers*, 9(4), 1163–1177, https://doi.org/10.1016/j.gsf.2018.01.006.
- Harland, W. B. (1971), Tectonic transpression in Caledonian Spitsbergen, Geological Magazine, 108(1), 27–41, https://doi.org/10.1017/s0016756800050937.
- Hauteville, A., A.-S. André-Mayer, A. Eglinger, J. Perret, T. Nobilet, Y. Teitler, B. Touré, L. Ciancaleoni, L. Marulier, and Y. Coulibaly (2025), Tourmaline as a textural, geochemical and isotopic marker of fault valve processes recorded at the Paleoproterozoic Lafigué orogenic gold deposit, Ivory Coast, *Mineralium Deposita*, 60(6), 1297–1324, https://doi.org/10.1007/s00126-024-01335-7.
- Hayman, P. C., P. Bolz, G. Senyah, E. Tegan, S. Denyszyn, D. T. Murphy, and M. W. Jessell (2023), Physical and geochemical reconstruction of a 2.35–2.1 Ga volcanic arc (Toumodi Greenstone Belt, Ivory Coast, West Africa), Precambrian Research, 389(107029), 107,029, https://doi.org/10.1016/j.precamres.2023.107029.
- Hirth, G., and J. Tullis (1992), Dislocation creep regimes in quartz aggregates, Journal of Structural Geology, 14(2), 145–159, https://doi.org/10.1016/0191-8141(92)90053-y.
- Hodgson, C. J. (1989), The structure of shear-related, vein-type gold deposits: A review, Ore Geology Reviews, 4(3), 231–273, https://doi.org/10.1016/0169-1368(89)900 19-x.
- Holdsworth, R. E., C. A. Butler, and A. M. Roberts (1997), The recognition of reactivation during continental deformation, *Journal of the Geological Society*, 154(1), 73–78, https://doi.org/10.1144/gsjgs.154.1.0073.
- Jébrak, M., and E. Marcoux (2008), Géologie des ressources minérales, Ministère des ressources naturelles et de la faune Avenue Ouest, QC, Canada.

- Kamb, W. B. (1959), Ice petrofabric observations from Blue Glacier, Washington, in relation to theory and experiment, *Journal of Geophysical Research*, 64(11), 1891–1909, https://doi.org/10.1029/JZ064I011P01891.
- Kennedy, W. Q. (1964), The structural differentiation of Africa in the Pan-African (±500 m.y.) tectonic episode, Annual Report of the Research Institute of African Geology, pp. 48–49.
- Koffi, A. Y., N. Thébaud, A. N. Kouamelan, L. Baratoux, O. Bruguier, O. Vanderhaeghe, P. Pitra, A. I. S. Kemp, and N. J. Evans (2022), Archean to Paleoproterozoic crustal evolution in the Sassandra-Cavally domain (Côte d'Ivoire, West Africa): Insights from Hf and U-Pb zircon analyses, *Precambrian Research*, 382(106875), 106,875, https://doi.org/10.1016/j.precamres.2022.106875.
- Kouamelan, A., C. Delor, and J. Peucat (1997), Geochronological evidence for reworking of Archean terrains during the Early Proterozoic (2.1 Ga) in the western Co^te d'Ivoire (Man Rise-West African Craton), Precambrian Research, 86(3-4), 177–199, https://doi.org/10.1016/S0301-9268(97)00043-0.
- Kouamelan, A., S. C. Djro, M. E. Allialy, J. Paquette, and J. Peucat (2015), The oldest rock of Ivory Coast, *Journal* of African Earth Sciences, 103, 65–70, https://doi.org/10 .1016/J.JAFREARSCI.2014.12.004.
- Krantz, R. W. (1995), The transpressional strain model applied to strike-slip, oblique-convergent and oblique-divergent deformation, *Journal of Structural Geology*, 17(8), 1125–1137, https://doi.org/10.1016/0191-8141(94)00129-n.
- Lacroix, B., J. Hughes, A. Lahfid, J. E. Spangenberg, B. Putlitz, C. Ward, N. Niemi, and P. D. Kempton (2020), Structure and origin of the gold mineralization in the Nacimiento Block: The Los Burros deposits (Central California), Ore Geology Reviews, 125(103668), 103,668, https://doi.org/10.1016/j.oregeorev.2020.103668.
- Lawley, C., J. Imber, and D. Selby (2013), Structural controls on orogenic Au mineralization during transpression: Lupa goldfield, southwestern Tanzania, *Economic Geology and the Bulletin of the Society of Economic Geologists*, 108(7), 1615–1640, https://doi.org/10.2113/econgeo.108.7.1615.
- Leever, K. A., R. H. Gabrielsen, D. Sokoutis, and E. Willingshofer (2011), The effect of convergence angle on the kinematic evolution of strain partitioning in transpressional brittle wedges: Insight from analog modeling and high-resolution digital image analysis: KINEMATICS OF STRAIN PARTITIONING, Tectonics, 30(2), 2010TC002,823, https://doi.org/10.1029/2010tc002823
- Lloyd, G., and B. Freeman (1994), Dynamic recrystallization of quartz under greenschist conditions, *Journal of Structural Geology*, 16(6), 867–881, https://doi.org/10.1016/0191-8141(94)90151-1.
- Martin-Izard, A., D. Arias, M. Arias, P. Gumiel, D. J. Sanderson, C. Castañon, and J. Sanchez (2016), Ore deposit types and tectonic evolution of the Iberian Pyrite Belt: From transtensional basins and magmatism to transpression and inversion tectonics, Ore Geology Reviews, 79, 254–267, https://doi.org/10.1016/j.oregeo

rev.2016.05.011.

- Martín-Izard, A., A. Arribas, D. Arias, J. Ruiz, and F. J. Fernández (2002), The Fe deposit, west-central Spain: Tectonic-hydrothermal uranium mineralization associated with transpressional faulting of alpine age, The Canadian Mineralogist, 40(5), 1505–1520, https://doi.org/10.2113/ GSCANMIN. 40.5.1505.
- Masurel, Q., A. Eglinger, N. Thébaud, A. Allibone, A.-S. André-Mayer, H. McFarlane, J. Miller, M. Jessell, L. Aillères, O. Vanderhaeghe, S. Salvi, L. Baratoux, S. Perrouty, G. Begg, D. Fougerouse, P. Hayman, O. Wane, A. Tshibubudze, L. Parra-Avila, A. Kouamélan, and P. O. Amponsah (2022), Paleoproterozoic gold events in the southern West African Craton: review and synopsis, Mineralium Deposita, 57(4), 513-537, https://doi.org/ 10.1007/s00126-021-01052-5.
- Micklethwaite, S., H. A. Sheldon, and T. Baker (2010), Active fault and shear processes and their implications for mineral deposit formation and discovery, Journal of Structural Geology, 32(2), 151–165, https://doi.org/10.1016/j.jsg. 2009.10.009.
- Micklethwaite, S., A. Ford, W. Witt, and H. A. Sheldon (2015), The where and how of faults, fluids and permeability - insights from fault stepovers, scaling properties and gold mineralisation, Geofluids, 15(1-2), 240–251, https://doi.org/10.1111/gfl.12102.
- Miller, L. D., H. H. Stowell, and G. E. Gehrels (2000), Progressive deformation associated with mid-Cretaceous to Tertiary contractional tectonism in the Juneau gold belt, Coast Mountains, southeastern Alaska, in Tectonics of the Coast Mountains, Southeastern Alaska and British Columbia, Geological Society of America, https://doi.org/ 10.1130/0-8137-2343-4.193.
- Miller, M. G. (2014), 4 · Kinematic Indicators in Brittle Fault Zones, in Fault-related Rocks, pp. 30–31, Princeton University Press.
- Miller, R. B. (1994), A mid-crustal contractional stepover zone in a major strike-slip system, North Cascades, Washington, Journal of Structural Geology, 16(1), 47-60, https://doi.org/10.1016/0191-8141(94)90017-5.
- Mériaud, N., N. Thébaud, Q. Masurel, P. Hayman, M. Jessell, A. Kemp, N. J. Evans, C. M. Fisher, and P. M. Scott (2020), Lithostratigraphic evolution of the Bandamian Volcanic Cycle in central Côte d'Ivoire: Insights into the late Eburnean magmatic resurgence and its geodynamic implications, Precambrian Research, 347 (105847), 105,847, https://doi.org/10.1016/j.precamres.2020.105847.
- Nabavi, S. T., S. A. Alavi, S. Mohammadi, M. R. Ghassemi, and M. Frehner (2017), Analysis of transpression within contractional fault steps using finite-element method, Journal of Structural Geology, 96, 1-20, https://doi.or g/10.1016/J.JSG.2017.01.004.
- Nevitt, J. M., D. D. Pollard, and J. M. Warren (2014), Evaluation of transfersion and transpression within contractional fault steps: Comparing kinematic and mechanical models to field data, Journal of Structural Geology, 60, 55-69, https://doi.org/10.1016/j.jsg.2013 .12.011.

- Okazaki, K., and H. Conrad (1972), Grain size distribution in recrystallized alpha-titanium, Transactions of the Japan Institute of Metals, 13(3), 198–204, https://doi.org/10.2 320/MATERTRANS1960.13.198.
- Oliver, N. H. S., and P. D. Bons (2001), Mechanisms of fluid flow and fluid-rock interaction in fossil metamorphic hydrothermal systems inferred from vein-wallrock patterns, geometry and microstructure, Geofluids, 1(2), 137–162, https://doi.org/10.1046/j.1468-8123.2001.00013
- Ouattara, G. (1998), Structure du batholite Ferkéssédougou (secteur de Zuénoula, Côte d'Ivoire), Ph.D. thesis, Université d'Orléans, ISTO, Orléans, France.
- Papa, S., G. Pennacchioni, L. Menegon, and M. Thielmann (2020), High-stress creep preceding coseismic rupturing in amphibolite-facies ultramylonites, Earth and Planetary Science Letters, 541(116260), 116,260, https://doi.org/10 .1016/j.epsl.2020.116260.
- Passchier, C. W., and R. A. J. Trouw (2005), Shear Zones, in *Microtectonics*, 2nd edition ed., pp. 111–158, Springer-Verlag, Berlin/Heidelberg, https://doi.org/10.1 $007/3-540-29359-0_5.$
- Peacock, D. C. P., and D. J. Sanderson (1995), Strike-slip relay ramps, Journal of Structural Geology, 17(10), 1351-1360, https://doi.org/10.1016/0191-8141(95)973 0.3 - w
- Perret, J. (2025), GEOL-QMAPS (QGIS-based solution for digital geological mapping), https://doi.org/10.5281/ZE NODO.14823224.
- Perret, J., J. Feneyrol, A. Eglinger, A.-S. André-Mayer, C. Berthier, A. Ennaciri, and R. Bosc (2021), Tectonic record and gold mineralization in the central part of the Neoproterozoic Keraf suture, Gabgaba district, NE Sudan, Journal of African Earth Sciences, 181(104248), 104,248, https://doi.org/10.1016/j.jafrearsci.2021.104248.
- Perret, J., M. W. Jessell, and E. Bétend (2024), An open-source, QGIS-based solution for digital geological GEOL-QMAPS, Applied Computing and Geosciences, 24(100197), 100,197, https://doi.org/10.1 016/j.acags.2024.100197.
- Perret, J., M. W. Jessell, Q. Masurel, P. C. Hayman, N. Thébaud, L. Baratoux, A. Kouamélan, A. Eglinger, A.-S. André-Mayer, A. Y. Koffi, I. Dia, J. Koné, J. Davis, O. Wane, P. O. Amponsah, S. Naba, and O. Vanderhaeghe (2025), Review of Paleoproterozoic tectonics in the southern West African Craton: Insights from multi-disciplinary data integration, Precambrian Research, 422(107707), 107,707, https://doi.org/10.101 6/j.precamres.2025.107707.
- Perrouty, S., L. Aillères, M. W. Jessell, L. Baratoux, Y. Bourassa, and B. Crawford (2012), Revised Eburnean geodynamic evolution of the gold-rich southern Ashanti Belt, Ghana, with new field and geophysical evidence of pre-Tarkwaian deformations, Precambrian Research, 204-205, 12-39, https://doi.org/10.1016/j.precamres. 2012.01.003.
- S. G. (1993), Nomenclature, concepts and Peters. classification of oreshoots in vein deposits, Ore Geology

- Reviews, 8(1-2), 3-22, https://doi.org/10.1016/0169-136 8(93)90025-t.
- Platt, J. P., and W. M. Behr (2011), Grainsize evolution in ductile shear zones: Implications for strain localization and the strength of the lithosphere, Journal of Structural Geology, 33(4), 537–550, https://doi.org/10.1016/j.jsg.20 11.01.018.
- Ramsay, J. G., and M. I. Huber (1987), Modern structural geology, Folds and Fractures, 2, 309-700.
- Robert, F., A. Boullier, and K. Firdaous (1995), Gold-quartz veins in metamorphic terranes and their bearing on the role of fluids in faulting, Journal of Geophysical Research, Solid Earth, 100(B7), 12,861–12,879, https://doi.org/10.1 029/95JB00190.
- Rutter, E. H., R. E. Holdsworth, and R. J. Knipe (2001), The nature and tectonic significance of fault-zone weakening: an introduction, Geological Society Special Publication, 186(1), 1–11, https://doi.org/10.1144/GSL.SP.2001.18 6.01.01.
- Sanderson, D. J., and W. R. D. Marchini (1984), Transpression, Journal of Structural Geology, 6(5), $449-458,\ https://doi.org/10.1016/0191-8141(84)90058-0.$
- Seymour, N. M., J. S. Singleton, R. Gomila, G. Arancibia, J. Ridley, M. L. Gevedon, D. Stockli, and S. M. Seman (2024), Sodic-calcic alteration and transpressional shear along the Atacama fault system during IOCG mineralization, Copiapó, Chile, Mineralium Deposita, pp. 1-29, https://doi.org/10.1007/s00126-024-01259-2.
- Shigematsu, N., D. J. Prior, and J. Wheeler (2006), First combined electron backscatter diffraction and transmission electron microscopy study of grain boundary structure of deformed quartzite, Journal of Microscopy, 224(3), 306-321, https://doi.org/10.1111/J.1365-2818.2006.0 1697.X.
- Sibson, R. (1990), Conditions for fault-valve behaviour, Geological Society Special publication, 54(1), 15–28, https: //doi.org/10.1144/GSL.SP.1990.054.01.02.
- Sibson, R. (2001), Seismogenic framework for hydrothermal transport and ore deposition, in Structural Controls on Ore Genesis, Reviews in Economic Geology, vol. 14, edited by J. P. Richards and R. M. Tosdal, pp. 25-50, Society of Economic Geologists, https://doi.org/10.5382/rev.14.02.
- Sibson, R. (2004), Controls on maximum fluid overpressure defining conditions for mesozonal mineralisation, Journal of Structural Geology, 26(6-7), 1127–1136, https://doi.or g/10.1016/J.JSG.2003.11.003.
- Sibson, R., and J. Scott (1998), Stress/fault controls on the containment and release of overpressured fluids: Examples from gold-quartz vein systems in Juneau, Alaska; Victoria, Australia and Otago, New Zealand, Ore Geology Reviews, 13(1-5), 293-306, https://doi.org/10.1016/S0169-1368(97)00023-1.
- Sibson, R. H. (1981), Fluid flow accompanying faulting: field evidence and models, in Earthquake Prediction: An International Review, vol. 4, pp. 593–603, American Geophysical Union (AGU), https://doi.org/10.1029/ME 004p0593.

- Sibson, R. H. (1992), Fault-valve behavior hydrostatic-lithostatic fluid pressure interface, Earth-Science Reviews, 32(1-2), 141–144, https: //doi.org/10.1016/0012-8252(92)90019-p.
- Sibson, R. H. (1996), Structural permeability of fluid-driven ${\it fault-fracture meshes},\, Journal\,\, of\, Structural\,\, Geology,\, 18 (8),$ 1031-1042, https://doi.org/10.1016/0191-8141(96)00032
- Sibson, R. H. (2020), Preparation zones for large crustal earthquakes consequent on fault-valve action, Earth, Planets and Space, 72(1), https://doi.org/10.1186/s406 23-020-01153-x.
- Solar, G. S., and M. Brown (2001), Deformation partitioning during transpression in response to Early Devonian oblique convergence, northern Appalachian orogen, USA, Journal of Structural Geology, 23(6-7), 1043–1065, https://doi.or g/10.1016/s0191-8141(00)00175-9.
- Stipp, M., and K. Kunze (2008), Dynamic recrystallization the brittle-plastic transition in experimentally deformed quartz aggregates, Tectonophysics, 448(1-4), 77-97, https://doi.org/10 .1016/j.tecto.2007.11.041.
- Stipp, M., H. Stünitz, R. Heilbronner, and S. M. Schmid (2002a), The eastern Tonale fault zone: a 'natural laboratory' for crystal plastic deformation of quartz over a temperature range from 250 to 700°C, Journal of Structural Geology, 24(12), 1861–1884, https://doi.org/10.1016/s019 1-8141(02)00035-4.
- Stipp, M., H. Stünitz, R. Heilbronner, and S. M. Schmid (2002b), Dynamic recrystallization of quartz: correlation between natural and experimental conditions, Geological Society Special Publication, 200(1), 171–190, https://doi. org/10.1144/GSL.SP.2001.200.01.11.
- Tikoff, B., and C. Teyssier (1994), Strain modeling of displacement-field partitioning in transpressional orogens, Journal of Structural Geology, 16(11), 1575–1588, https: //doi.org/10.1016/0191-8141(94)90034-5.
- Torgersen, E., and G. Viola (2014), Structural and temporal evolution of a reactivated brittle-ductile fault - Part I: Fault architecture, strain localization mechanisms and deformation history, Earth and Planetary Science Letters, 407, 205–220, https://doi.org/10.1016/j.epsl.2014.09.019.
- Tornos, F., C. Casquet, and J. M. R. S. Relvas (2005), 4: Transpressional tectonics, lower crust decoupling and intrusion of deep mafic sills: A model for the unusual metallogenesis of SW Iberia, Ore Geology Reviews, 27(1-4), 133–163, https://doi.org/10.1016/j.oregeorev.2005.07.020.
- Traoré, K., D. Chardon, S. Naba, O. Wane, and M. L. Bouaré (2022), Paleoproterozoic collision tectonics in West Africa: Insights into the geodynamics of continental growth, Precambrian Research, 376(106692), 106,692, ht tps://doi.org/10.1016/j.precamres.2022.106692.
- Trimby, P., D. Prior, and J. Wheeler (1998), Grain boundary hierarchy development in a quartz mylonite, Journal of Structural Geology, 20(7), 917–935, https://doi.org/10.1 016/S0191-8141(98)00026-1.
- Twiss, R. J. (1977), Theory and applicability of a recrystallized grain size paleopiezometer, Pure and Applied

- Geophysics, 115, 227–244, https://doi.org/10.1007/BF01 637105.
- Urai, J. L., P. F. Williams, and H. L. M. Van Roermund (1991), Kinematics of crystal growth in syntectonic fibrous veins, Journal of Structural Geology, 13(7), 823–836.
- Wane, O., J.-P. Liégeois, N. Thébaud, J. Miller, V. Metelka, and M. Jessell (2018), The onset of the Eburnean collision with the Kenema-Man craton evidenced by plutonic and volcanosedimentary rock record of the Masssigui region, southern Mali, Precambrian Research, 305, 444-478, https:// //doi.org/10.1016/j.precamres.2017.11.008.
- Weedon, P., E. Chapman, R. Espinoza, M. Veillette, and P. Criddle (2023), Fortuna Silver Mines Inc: Séguéla Gold Mine, Côte d'Ivoire, Tech. rep., Fortuna Silver Mines Inc.
- Westaway, R. (1995), Deformation around stepovers in strike-slip fault zones, Journal of Structural Geology, 17(6), 831-846, https://doi.org/10.1016/0191-8141(94)00098-k.
- Wheeler, J., Z. Jiang, D. J. Prior, and J. Tullis (2004), Dynamic Recrystallisation of Quartz, Materials Science Forum, 467-470, 1243-1250, https://doi.org/10.4028/ww w.scientific.net/msf.467-470.1243.
- White, J., and S. White (1981), On the structure of grain boundaries in tectonites, Tectonophysics, 78(1-4), 613-628, https://doi.org/10.1016/0040-1951(81)90032-9.
- White, S. (1977), Geological significance of recovery and recrystallization processes in quartz, Tectonophysics, 39(1-3), 143–170, https://doi.org/10.1016/0040-1951(77)9 0093 - 2.
- Worley, B. A., and C. J. L. Wilson (1996), Deformation partitioning and foliation reactivation during

- transpressional orogenesis, an example from the Central Longmen Shan, China, Journal of Structural Geology, 18(4), 395–411, https://doi.org/10.1016/0191-8141(95)0 0095-u.
- Wright, S., M. Nowell, and D. Field (2011), A review of strain analysis using electron backscatter diffraction, Microscopy and Microanalysis, 17(3), 316-329, https://doi.org/10.101 7/S1431927611000055.
- Wu, Y., J. Zhang, B. Zhang, X. Mao, Z. Lu, G. Zhou, X. Teng, and Q. Guo (2023), Early Paleozoic oblique convergence from subduction to collision: Insights from timing and structural style of the transpressional dextral shear zone in the Qilian orogen, northern Tibet of China, Geological Society of America Bulletin, https://doi.org/10 .1130/b36947.1.
- Xia, H., and J. P. Platt (2018), Quartz grainsize evolution during dynamic recrystallization across a natural shear zone boundary, Journal of Structural Geology, 109, 120–126, https://doi.org/10.1016/j.jsg.2018.01.007.
- Yan, Q., X. Jiang, W. Li, C. Li, and F. Yang (2024), Genesis of alkaline porphyries and associated Cu-Au-Pb-Ag polymetallic mineralization in an intracontinental transpression setting: Example from the Yao'an volcano-plutonic complex in western Yangtze Craton, SW China, Ore Geology Reviews, p. 105922, https://doi.org/10.1016/j.oregeorev.2024.105922.
- Zoheir, B. (2011), Transpressional zones in ophiolitic mélange terranes: Potential exploration targets for gold in the South Eastern Desert, Egypt, Journal of Geochemical Exploration, 111(1-2), 23-38, https://doi.org/10.1016/ j.gexplo.2011.07.003.